CrystEngComm

STRUCTURAL CHEMISTRY OF PENTA- AND HEXANITRATO THORIUM(IV) COMPLEXES ISOLATED USING N-H DONORS

Journal:	*CrystEngComm*
Manuscript ID	CE-ART-12-2023-001319.R1
Article Type:	Paper
Date Submitted by the Author:	30-Jan-2024
Complete List of Authors:	Shore, Madeline; Georgetown University, Department of Chemistry Nicholas, Aaron; The Pacific Northwest National Laboratory Vasiliu, Monica; The University of Alabama, Chemistry Edwards, Kyle; The University of Alabama, Chemistry de Melo, Gabriel; The University of Alabama, Chemistry Bertke, Jeffery; Georgetown University, Department of Chemistry Dixon, David; The University of Alabama, Chemistry Knope, Karah; Georgetown University, Department of Chemistry

STRUCTURAL CHEMISTRY OF PENTA- AND HEXANITRATO THORIUM(IV) COMPLEXES ISOLATED USING N-H DONORS

Madeline C. Shore,[1] Aaron D. Nicholas,[2] Monica Vasiliu,[3] Kyle C. Edwards,[3] Gabriel F. de Melo,[3] Jeffery A. Bertke,[1] David A. Dixon,[3] and Karah E. Knope[1,]*

[1] Department of Chemistry, Georgetown University, Washington, D.C. 20057, United States of America
[2] Pacific Northwest National Laboratory, 902 Battelle Boulevard, Richland, WA, 99354, United States of America
[3] Department of Chemistry and Biochemistry, The University of Alabama, Tuscaloosa, Alabama 35487, United States of America

KEYWORDS
THORIUM • STRUCTURAL CHEMISTRY • SUPRAMOLECULAR INTERACTIONS • ELECTRONIC STRUCTURE CALCULATIONS • ELECTROSTATIC POTENTIAL SURFACES

ABSTRACT
A series of fifteen tetravalent thorium phases were prepared. The compounds were isolated from acidic aqueous nitrate solutions using protonated nitrogen heterocycles of varying hydrogen-bond donation strength. Structural analysis via single crystal X-ray diffraction showed that the structures are built from pentanitrato, $[Th(NO_3)_5(H_2O)_2]^{1-}$, and hexanitrato, $[Th(NO_3)_6]^{2-}$, molecular units, with the latter being far more prevalent in the solid-state. The vibrational properties of the compounds were examined using Raman and IR spectroscopy; the spectra are dominated by stretches characteristic of nitrate and the organic ions. The relative energetics of nitrate complexation was examined using electronic structure theory. These results confirmed that there are clear thermodynamic sinks for the penta- and hexanitrato structural units that were observed experimentally. Additionally, electrostatic surface potentials (ESPs) were calculated in an effort to better understand the counterion stabilization of the complexes. The ESP surfaces showed that the position of the water and nitrate molecules and the coordination geometry of the metal complex had a clear effect on the polarizability of the two structural motifs. Despite limited speciation of the Th-nitrate structural units, the compounds exhibit rich supramolecular chemistry resulting from hydrogen bonding of the Th complexes with the organic N-H donors and π-π stacking interactions from the protonated N-heterocycles.

INTRODUCTION

Structural chemistry has played an important role in our understanding of the chemical and physical behavior of the actinides. Elucidating how 5f metal ions speciate – the complexes that are formed and how they transform – is critical to advancing nuclear energy systems, managing spent fuel inventories, and altogether predicting actinide fate under chemically complex conditions.[1–4] Indeed, such recognition as well as the application of these elements to areas ranging from biomedicine[5,6] to quantum information science[7] has motivated research efforts centered on actinide structural chemistry, bonding, and reactivity.[8–14]

In aqueous systems, actinide speciation is principally governed by oxidation state.[2–4] Whereas thorium exists near exclusively as a tetravalent metal ion in water, uranium, neptunium, and plutonium have multiple accessible oxidation states, with the higher valent ions forming 'yl' complexes and the lower valent ions adopting more spherical coordination geometries.[15] These differences alone dispose the lower- and higher- valent actinides to varied coordination chemistries

and hence metal-ligand complexation. Additionally, the increased charge density of the An^{4+} ions relative to the AnO_2^{2+} units, for example, result in a greater propensity of the 4+ metal ions to hydrolyze, with solution conditions playing a significant role in the degree to which such behavior is observed.[15,16] Thus in addition to oxidation state, it is well established that the concentration and identity of inner sphere ligands as well as experimental conditions impact actinide-ligand bonding and structure.

More recent work across the d- and f-block has shown that outer coordination sphere interactions likewise warrant consideration.[17–23] Noncovalent interactions such as ion-pairing have been shown to direct structure,[18] shift redox potentials,[23,24] and affect properties such as the extraction behavior of metal ions.[25,26] With this in mind, our group has been examining the effects of outer sphere interactions on actinide solid-state structural chemistry.[27–30] We previously reported a series of Th-aquo-chloro complexes, where the identity of the solid-state structural unit and the chloride distribution about the metal center, in particular, had some dependence on the pK_a of the N-heterocycle employed.[27] In an effort to further understand the influence of counterions on actinide speciation, we have looked to other monoanionic ligand systems that similarly form relatively weak Th complexes.[28]

Thorium remains our metal of choice for this work as it is stable under ambient conditions, is redox-inactive, is the least susceptible to hydrolysis and condensation, and can adopt a range of accessible coordination numbers. As a hard Lewis acid, thorium 4+ forms stronger complexes with harder ions; this is reflected in the formation constants for Th-F^{3+} (8.87) and Th-Cl^{3+} (1.70).[31] Nitrate also forms relatively weak, soluble complexes with thorium and thus, like chloride, should permit competition with water; the stability constant for the formation of $ThNO_3^{3+}$ is 1.30.[31] However, the coordination chemistry is characterized by a bidentate coordination mode and as evidenced by previous examinations of Th-nitrate structural chemistry may result in a smaller range of potential structural units.[18,32] The similarity in anion charge but the difference in complexation behavior provides an impetus for extending our efforts to nitrate ligand systems. Moreover, nitrates are relevant to both nuclear waste reprocessing and environmental systems and further motivates our interest in this area.[33]

In this work, the synthesis and solid-state structural chemistry of Th-nitrate complexes prepared in the presence of twelve N-heterocycles capable of H-bond donation (Scheme 1) were examined. Fifteen compounds were synthesized, and structural analysis showed the isolation of two unique structural units of the general formulas $[Th(NO_3)_6]^{2-}$ and $[Th(NO_3)_5(H_2O)_2]^{1-}$. Despite these common structural motifs, significant differences were observed in the noncovalent interaction strength and resulting supramolecular networks. Electronic structure theory was used to examine the relative energetics of nitrate complexation, and electrostatic surface potentials (ESPs) were calculated in an effort to better understand the counterion stabilization of the complexes. Consistent with our solid-state observations, these results show that there are clear thermodynamic driving forces for precipitation of the penta- and hexa-nitrato structural units, with the N-H donors playing an important role in the isolation of anionic units.

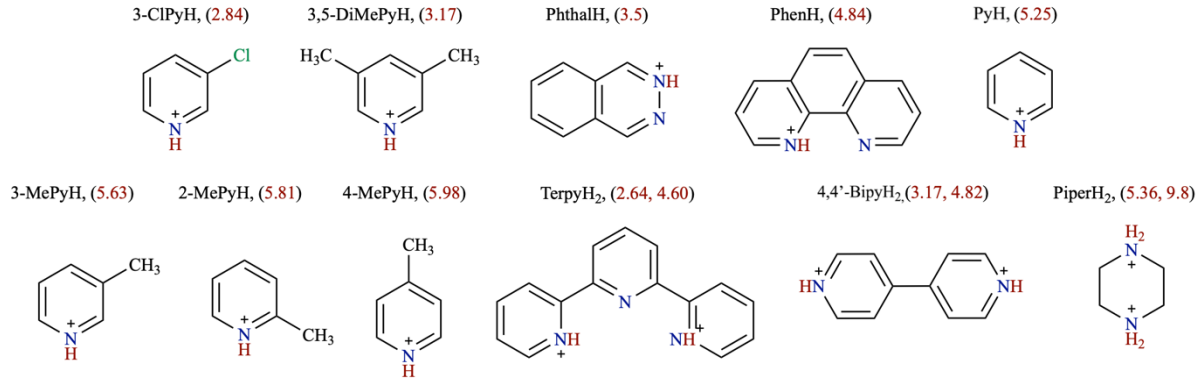

Scheme 1 Chemical structures of the protonated nitrogen-containing heterocycles used in this work and their corresponding pK_a[34] values.

EXPERIMENTAL METHODS

Syntheses.

Caution: ^{232}Th is an α-emitting radionuclide and standard precautions for handling radioactive materials should be followed. The following chemicals were used as received from commercial suppliers: thorium(IV) nitrate (International Bio- Analytical Industries, Inc.), 2-methylpyridine (2-MePy; Merck), 1,10-phenanthroline (Phen; Acros Organics, 99+%), 2,2′:6′,2″-terpyridine (Terpy; Acros Organics, 96%), 4,4′-bipyridine (4,4′-Bipy; Chem-Impex), 3-chloropyridine (3-ClPy; Alfa Aesar), piperazine (piper; Sigma-Aldrich 99%), 3,5-dimethylpyridine (3,5-DiMePy; Acros Organics, 98+%), 4-methylpyridine (4-MePy; Merck), 3-methylpyridine (3-MePy; Acros Organics, 99+%), pyridine (Py; Sigma-Aldrich 99%) and phthalazine (Phthal; Alfa Aesar). Water was purified by a Millipore Direct-Q 3UV water purification system; concentrated nitric acid (HNO_3, Fisher Chemical) was diluted into nanopure water (≤0.05 μS).

Fifteen compounds were prepared following a general synthetic procedure that employed either solvent layering and/or solvent evaporation.

Compounds $(PiperH_2)[Th(NO_3)_5(H_2O)_2]_2$•$[PiperH_2(NO_3)_2]$ (**1**), $(TerpyH_2)[Th(NO_3)_5(H_2O)_2]2$•$[(TerpyH_2)_3(NO_3)_6]$•$4(H_2O)$ (**2**), $(PyH)_2[Th(NO_3)_6]$•$(PyH•NO_3)$ (**3**), $(4,4'\text{-}BipyH_2)_2[Th(NO_3)_6]_2$•$[4,4'\text{-}BipyH_2•2NO_3]$ (**9**), $(PhthalH)_2[Th(NO_3)_6]$ (**10**), $(PhenH)_2[Th(NO_3)_6]•2H_2O$ (**15**), were synthesized via solvent layering. Thorium nitrate (0.048g, 0.1 mmol) was dissolved into 1M $HNO_{3(aq)}$ (500 μL) in a glass vial (3 mL) to form an acidic 0.25 M Th^{IV} solution. A separate solution was prepared by dissolving the respective N-heterocycle (0.1 mmol) into 1-hexanol (500 μL). The resulting solutions were then layered. Vials were left uncapped in a fume hood.

Compounds $(TerpyH_2)[Th(NO_3)_6]$•$(TerpyH_2)(NO_3)_2$ (**7**), $(4\text{-}MePyH)_2[Th(NO_3)_6]$ (**8**), $(3\text{-}MePyH)_2[Th(NO_3)_6]$ (**13**), were prepared via evaporation of an acidic aqueous solution. Thorium nitrate (0.048g, 0.1 mmol) was dissolved into 1M $HNO_{3(aq)}$ (500 μL). The respective N-heterocycle (0.1 mmol) was added, and the resulting was then left to slowly evaporate under a nitrogen atmosphere. Note that a nitrogen atmosphere was employed for greater control over the evaporation rate and to facilitate crystallization.

Compounds $(PyH)_2[Th(NO_3)_6]•2(PyH•NO_3)$ (**4**), $(3,5\text{-}DiMePyH)_2[Th(NO_3)_6]$•$[(3,5\text{-}DiMePyH)(NO_3)]$ (**5**), $(3,5\text{-}DiMePyH)_2[Th(NO_3)_6]$ (**6**), $(TerpyH_2)[Th(NO_3)_6]•H_2O$ (**11**), (2-

$MePyH)_2[Th(NO_3)_6]\bullet 2H_2O$ (**12),** $(3\text{-}ClPyH)_2[Th(NO_3)_6]$ (**14**), were prepared following the same general synthetic procedure as that described for **7**, **8**, and **13**; however, these phases were isolated from 3M $HNO_{3(aq)}$.

Colorless crystals of **1**–**15** were reproducibly observed after approximately 1-3 days. Crystals were mechanically separated from the bulk reaction products, with yields ranging from 12-46 %. Further details regarding the synthesis and phase purity as determined by powder X-ray diffraction (Figures S31-S45) are provided as Supplementary Information.

Structure Determination. The structures of **1-15** were determined via single-crystal X-ray diffraction. Single crystals were isolated from the bulk reaction products and mounted in mineral oil on MiTeGen micromounts. Data were collected at 100(2) K on a Bruker D8 Quest diffractometer equipped with a IμS X-ray source (Mo Kα radiation; λ = 0.71073) and a CMOS detector. The APEX III software suite was used to identify unit cells, integrate the data, and apply the absorption correction in SADABS.[35] The structures were solved using intrinsic phasing methods and refined using SHELXL within the ShelXle graphical user interface.[36] Crystallographic refinement details are provided in Table 1 and further details of the refinements are available as Supplementary Information.

Phase Purity. Powder X-ray diffraction data (Figures S31-S45) were collected on the reaction products from which single crystals were isolated to assess phase purity. Data were collected at room temperature using a DTeX Ultra Si strip detector from 3 to 40° 2θ on a Rigaku Ultima IV X-ray diffractometer with Cu Kα (λ = 1.541 Å) radiation.

Vibrational Spectroscopy. Raman spectra were collected on single crystals of **1**–**15** (Figures S46-S60) using a Horiba LabRAM HR Evolution Raman Spectrometer with an excitation line of 532 nm. Spectra were collected at room temperature over $\Delta\upsilon$ 200–4000 cm^{-1} using circularly polarized radiation. Infrared spectra of **1**–**15** were collected on samples consisting of several single crystals that were placed directly on a Nicolet iN10 Infrared Microscope FTIR-ATR stage with a Ge ATR tip. Spectra were collected at room temperature over $\Delta\upsilon$ 675–4000 cm^{-1} (Figures S46-S60).

Table 1. Crystallographic refinement details for compounds **1**–**15**.

	1	**2**	**3**	**4**	**5**
formula	$C_4H_{16}N_8O_{20}Th$	$C_{30}H_{34}N_{14}O_{29}Th$	$C_{15}H_{18}N_{10}O_{21}Th$	$C_{20}H_{24}N_{12}O_{24}Th$	$C_{10}H_{30}N_{10}O_{21}Th$
MW (g mol^{-1})	728.29	1270.75	906.43	1048.5	990.50
crystal color/ habit	colorless block	colorless block	colorless block	colorless block	colorless block
crystal system	triclinic	triclinic	monoclinic	monoclinic	monoclinic
space group	*P*2$_1$/*c*	*P-1*	*C 2/c*	*P 2$_1$/c*	*P*2$_1$/*c*
λ (Å)	0.71073	0.71073	0.71073	0.71073	0.71073
a (Å)	6.8020(5)	9.1818(8)	12.2065(10)	10.1866(7)	11.1786(9)
b (Å)	21.332(2)	15.7857(13)	12.3878(10)	13.3824(9)	18.1915(15)
c (Å)	13.2767(12)	16.523(2)	19.2532(16)	13.0890(9)	16.9407(14)
α (deg)	90	68.362(4)	90	90	90
β (deg)	97.576(3)	89.898(4)	108.057(2)	95.951(2)	93.437(3)
γ (deg)	90	75.320(2)	90	90	90
Volume (Å^3)	1909.6(3)	2142.2(4)	2767.9(4)	1774.7(2)	3438.8(5)
Z	4	2	4	2	4
ρ (mg m^{-3})	2.533	1.970	2.175	1.962	1.913
μ (mm^{-1})	7.931	3.599	5.501	4.312	4.436
R_1	0.0142	0.0231	0.0157	0.0178	0.0235
wR_2	0.0346	0.0417	0.0353	0.0485	0.0553
GOF	1.124	1.072	1.170	1.081	1.078
CCDC	2293425	2293426	2293427	2293428	2293429

	6	**7**	**8**	**9**	**10**
formula	$C_{14}H_{20}N_8O_{18}Th$	$C_{30}H_{26}N_{14}O_{24}Th$	$C_{12}H_{16}N_8O_{18}Th$	$C_{15}H_{15}N_{10}O_{21}Th$	$C_{16}H_{14}N_{10}O_{18}Th$
MW (g mol^{-1})	820.42	1198.69	792.37	903.41	866.41
crystal color/ habit	colorless block	Colorless block	colorless block	colorless block	colorless prism
crystal system	monoclinic	monoclinic	monoclinic	triclinic	monoclinic
space group	*P*2$_1$/*n*	*C 2/c*	*P*2$_1$/*n*	*P-1*	*C 2/c*
λ (Å)	0.71073	0.71073	0.71073	0.71073	0.71073
a (Å)	8.8462(6)	17.3812(15)	8.5991(5)	7.5205(3)	19.2301(9)
b (Å)	13.2604(9)	18.9121(15)	10.9119(6)	9.4305(4)	10.8154(5)
c (Å)	11.0517(7)	13.4970(11)	12.5427(7)	19.2896(8)	13.1377(6)
α (deg)	90	90	90	86.993(1)	90
β (deg)	101.802	113.819(3)	94.099(1)	83.564(1)	109.580(1)
γ (deg)	90	90	90	81.812(1)	90
Volume (Å^3)	1269.00(15)	4058.8(6)	1173.90(11)	1344.65(10)	2586.4(2)
Z	2	4	2	2	4
ρ (mg m^{-3})	2.147	1.962	2.242	2.231	2.225
μ (mm^{-1})	5.976	3.786	6.455	5.661	5.873
R_1	0.0180	0.0159	0.0151	0.0196	0.0208
wR_2	0.0399	0.0411	0.0352	0.0348	0.0409
GOF	1.078	1.122	1.208	1.029	1.015
CCDC	2293430	2293431	2293432	2293433	2293434

	11	**12**	**13**	**14**	**15**
formula	$C_{15}H_{15}N_9O_{19}Th$	$C_{12}H_{20}N_8O_{20}Th$	$C_{12}H_{16}N_8O_{18}Th$	$C_{10}H_{10}Cl_2N_8O_{18}Th$	$C_{24}H_{22}N_{10}O_{20}Th$
MW (g mol^{-1})	857.40	828.40	797.13	833.20	1002.56
crystal color/ habit	colorless block	colorless block	colorless block	colorless block	colorless block
crystal system	monoclinic	monoclinic	monoclinic	monoclinic	monoclinic
space group	*P2$_{1/n}$*	*C 2/c*	*C 2/c*	*C 2/c*	*P2$_1$/n*
λ (Å)	0.71073	0.71073	0.71073	0.71073	0.71073
a (Å)	10.0147(6)	19.2790(11)	14.0191(8)	13.9087(9)	7.5457(4)
b (Å)	21.9815(12)	10.3258(6)	13.8593(8)	13.7101(8)	14.7283(7)
c (Å)	11.6943(6)	13.1062(7)	12.6023(7)	12.6074(8)	14.8984(7)
α (deg)	90	90	90	90	90
β (deg)	97.889(2)	93.483(2)	101.727	101.770(2)	97.862(2)
γ (deg)	90	90	90	90	90
Volume (Å^3)	2550.0(2)	2604.3(3)	2397.5(2)	2356.6(3)	1640.18(14)
Z	4	4	4	4	2
ρ (mg m^{-3})	2.233	2.113	2.195	2.351	2.030
μ (mm^{-1})	5.957	5.830	6.332	6.665	4.650
R_1	0.0135	0.0129	0.0210	0.0136	0.0150
wR_2	0.0319	0.0342	0.0548	0.0346	0.0368
GOF	1.061	1.168	1.224	1.206	1.119
CCDC	2293435	2293436	2293437	2293438	2293439

Computational Methods

Electronic Structure Calculations. Details of the electronic structure calculations including the DFT/B3LYP/DZVP2 (H, N, O)/cc-pVDZ-PP(Th) geometry optimizations (DFT = density functional theory),[37–42] corrections to the entropy for low frequency modes,[43] single point CCSD(T) energy calculations with the same basis sets,[44–51] and solvation energy corrections (including a +4.3 kcal/mol correction per product H_2O),[52–54] are available as Supplementary Information.

Electrostatic Potential Surfaces. Noncovalent interactions between electron rich Th anionic units ($[ThNO_3)_6]^{2-}$) and $[Th(H_2O)_2(NO_3)_5]^{1-}$) and electron poor organic cationic H-donor units were explored using electrostatic potential surfaces (ESPs). Surfaces were generated on isolated ionic units that were optimized prior to surface generation using the DFT/B3LYP/DZVP2(H, N, O)/cc-pVDZ-PP(Th) approaches described above. Surfaces are rendered at 0.002 ε Bohr^{1-} with electron-rich and electron deficient areas highlighted. These methods have been used extensively by our group and others in previous reports.[27,55–58]

RESULTS AND DISCUSSION

Structure descriptions. Fifteen Th-nitrate bearing phases were isolated from acidic nitrate solutions using a series of eleven distinct N-H hydrogen bond donors. Overall, the compounds exhibit limited solid-state Th speciation, with only two structural units, $[Th(NO_3)_5(H_2O)_2]^{1-}$ $[Th(NO_3)_6]^{2-}$ (Figure 1), precipitating from solution. Average $Th–O_{H2O}$ and $Th–O_{NO3}$ bond distances for the pentanitrato complexes in **1-2** as well as the average $Th\text{-}NO_3$ distances for the hexanitrato units that constitute **3-15** are provided in Tables S3 and S4. Collectively, these structures exhibit rich noncovalent interactions including H-bonding and π-π stacking that give rise to supramolecular networks that range from 0-D to 3-D assemblies as summarized in Table 2. Brief descriptions of the supramolecular networks are provided herein, and full summaries of the

hydrogen bonding networks and π-π stacking interactions for each compound are provided in Tables S5-S19.

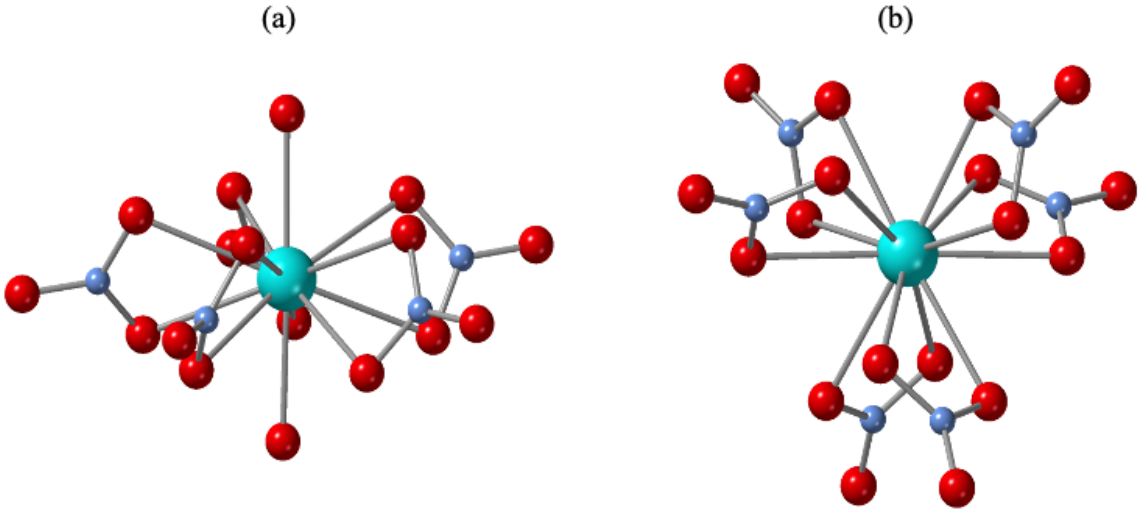

Figure 1. Illustration of the two distinct Th-nitrate structural units, $[Th(NO_3)_5(H_2O)_2]^{1-}$ (a) and $[Th(NO_3)_6]^{2-}$ (b) observed in **1-15**. The Th-hexanitrato building block is more prevalent in the solid state with thirteen phases exhibiting this motif. Teal spheres represent Th; red spheres are O, and blue sphere are nitrogen. Hydrogen atoms of the water molecules have been omitted for clarity.

Table 2. Summary of compounds **1-15**.

Compound	Formula	Dimensionality*
1	$(PiperH_2)[Th(NO_3)_5(H_2O)_2]_2$•$[PiperH_2(NO_3)_2]$	$2D^1$
2	$(TerpyH_2)[Th(NO_3)_5(H_2O)_2]_2$•$[(TerpyH_2)_3(NO_3)_6]$•$4(H_2O)$	$3D^{1,2}$
3	$(PyH)_2[Th(NO_3)_6]$•$(PyH$•$NO_3)$	$0D^{1,2}$
4	$(PyH)_2[Th(NO_3)_6]$•$2(PyH$•$NO_3)$	$0D^1$
5	$(3,5\text{-}DiMePyH)_2[Th(NO_3)_6]$•$[(3,5\text{-}DiMePyH)(NO_3)]$	$0D^1$
6	$(3,5\text{-}DiMePyH)_2[Th(NO_3)_6]$	$0D^1$
7	$(TerpyH_2)[Th(NO_3)_6]$•$(TerpyH_2)(NO_3)_2$	$0D^1$
8	$(4\text{-}MePyH)_2[Th(NO_3)_6]$	$1D^{1,2}$
9	$(4,4'\text{-}BipyH_2)_2[Th(NO_3)_6]_2$•$[4,4'\text{-}BipyH_2$•$2NO_3]$	$1D^1$
10	$(PhthalH)_2[Th(NO_3)_6]$	$1D^{1,2}$
11	$(TerpyH_2)[Th(NO_3)_6]$•H_2O	$1D^{1,2}$
12	$(2\text{-}MePyH)_2[Th(NO_3)_6]$•$2H_2O$	$2D^1$
13	$(3\text{-}MePyH)_2[Th(NO_3)_6]$	$2D^{1,2}$
14	$(3\text{-}ClPyH)_2[Th(NO_3)_6]$	$2D^{1,2}$
15	$(PhenH)_2[Th(NO_3)_6]$•$2[H_2O]$	$2D^{1,2}$

*Note that the dimensionality is defined based on propagation of the Th structural units. Supramolecular interactions are highlighted by superscript 1,2 with [1] denoting H-bonding interactions and [2] denoting compounds with π-π stacking.

Compounds built from $Th(NO_3)_5(H_2O)_2^{1-}$.

Compound **1**, $(PiperH_2)[Th(NO_3)_5(H_2O)_2]_2 \bullet [PiperH_2(NO_3)_2]$, crystallizes in the P $2_1/c$ space group. The structure is built from $[Th(NO_3)_5(H_2O)_2]^{1-}$ anionic units that are charged balanced by piperazinium cations. As shown in Figure 2a, the pentanitrato structural units are propagated into 2-dimensional sheets via H-bonding interactions that exist between the nitrate anions and water molecules of the $[Th(NO_3)_5(H_2O)_2]^{1-}$ complexes. Representative $O\text{-}H_{H2O}\text{---}O_{(NO3)}$ interaction distances and angles are 2.805(2) Å and 175(3)° respectively. The piperazinium cations reside in the outer coordination sphere (Figure 2b). These cations do not exhibit any significant noncovalent interactions with the Th structural units; however, do engage in H-bonding with free NO_3^{1-} anions ((N-H---O distance and angle of 2.796(2) Å and 167°; Figure 2b) to result in 2-dimensional sheets consisting of nitrate and piperazinium cations (Figure S16).

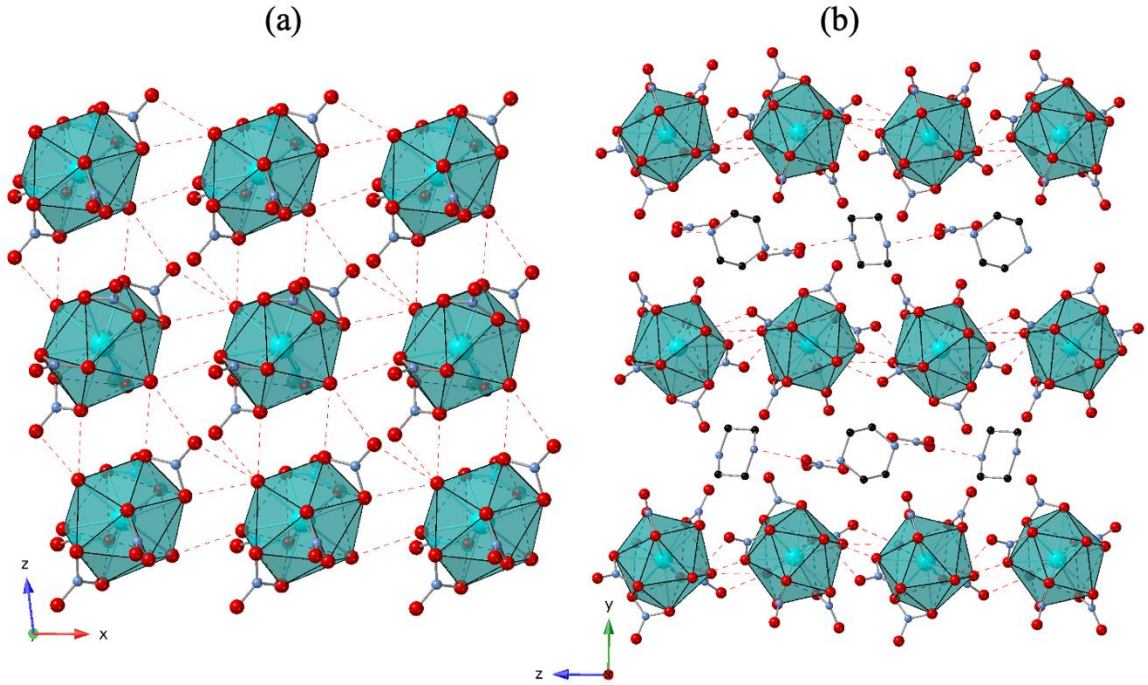

Figure 2. Packing diagram of **1**, $(PiperH_2)[Th(NO_3)_5(H_2O)_2]_2 \bullet [PiperH_2(NO_3)_2]$, viewed down (a) the [010] showing the 2-dimensional sheets that are formed through O-H---O H-bonding interactions between Th units (red dashed lines) and (b) the [100] highlighting alternating layers that consist of $[Th(NO_3)_5(H_2O)_2]^{1-}$ structural units and $[PiperH_2(NO_3)]^{1+}$. The latter is characterized by N-H---O H-bonding between the $PiperH_2$ cations and nitrate anions. Hydrogen atoms have been omitted for clarity. Color code: Th, teal; O, red; N, dark blue; C, black.

Compound **2**, $(TerpyH_2)[Th(NO_3)_5(H_2O)_2]_2$•$[(TerpyH_2)_3(NO_3)_6]$•$4(H_2O)$, crystallizes in the P-1 space group. The structure is built from $[Th(NO_3)_5(H_2O)_2]^{1-}$ anionic units that are charged balanced by terpyridinium cations. Overall, the structure adopts a 3-dimensional supramolecular network characterized by H-bonding and π–π stacking interactions. As shown in Figure 3a, extensive H-bonding exists between the water molecules and nitrate anions bound to the Th metal centers and the waters and nitrate ions that exist in the outer coordination sphere. Both the thorium bound water molecules and nitrate anions engage in H-bonding interactions to form 1D zig-zag chains that propagate along the [010] as shown in Figure 3a. Representative $O\text{-}H_{H2O}\text{---}O_{(NO3)}$ and N-H---O interaction distances are 2.638(3) and 2.681(4); the corresponding angles are 176(3)° and 167(3)° respectively. The terpyridinium cations reside in the outer coordination sphere (Figure 3b) and exhibit π-π stacking interactions that extend along the [100] (Figure 3c). The $C_{(terpy)}\text{---}C_{(terpy)}$ distance is 3.5299(18) Å and exhibits a slip angle of 13.1 °, consistent with a strong interaction.[59]

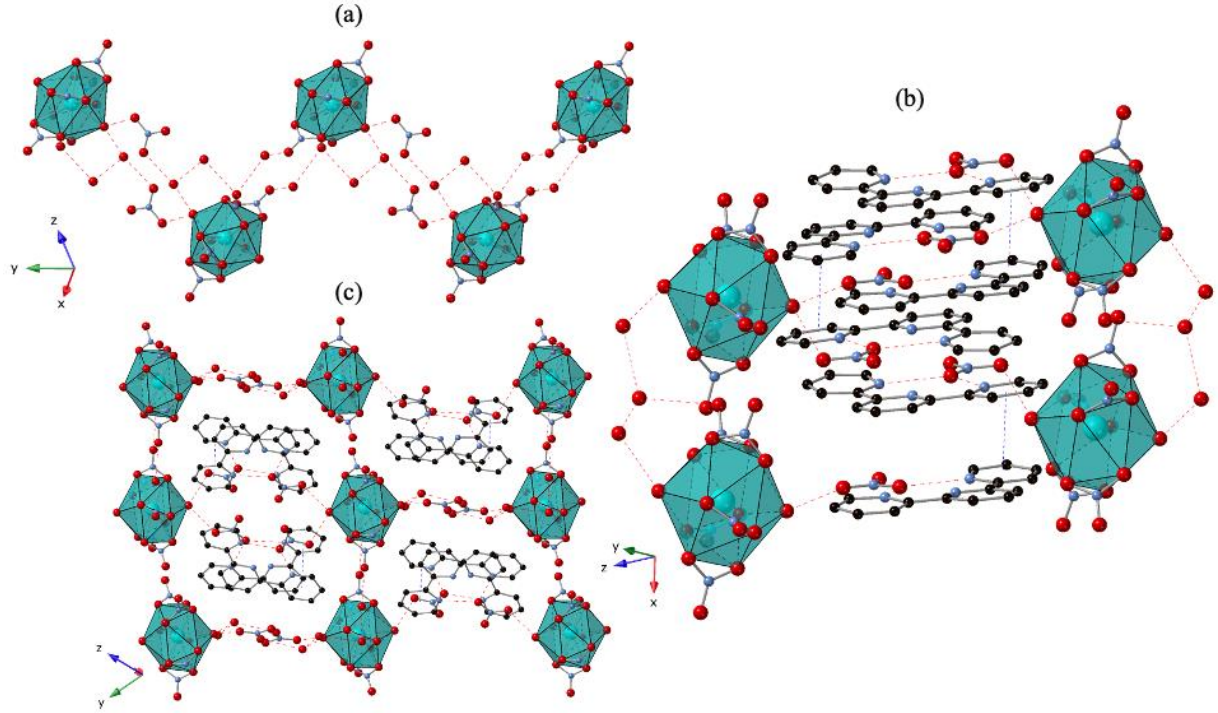

Figure 3. Illustration of the extended 3D supramolecular network of **2**, $(TerpyH_2)[Th(NO_3)_5(H_2O)_2]_2$•$[(TerpyH_2)_3(NO_3)_6]$•$4(H_2O)$. (a) $[Th(NO_3)_5(H_2O)_2]^{1-}$ units engage in H-bonding interactions with outer sphere water molecules and nitrate ions to yield 1-D zig-zag chains that propagate along the [010]. (b,c) The Th structural units are further connected along the [100] via H-bonding interactions. These interactions taken together with π-π stacking interactions between the terpyridinium cations results in an 3D supramolecular network. H-bonding and π-π stacking interactions are shown as red and blue dashed lines, respectively. Color code: Th, teal; O, red; N, dark blue; C, black. Hydrogen atoms have been omitted for clarity.

Compounds built from $[Th(NO_3)_6]^{2-}$.

Compound **3**, $(PyH)_2[Th(NO_3)_6]\bullet(PyH\bullet NO_3)$, crystallizes in the C2/c space group. The structure consists of $[Th(NO_3)_6]^{2-}$ anionic units that are charged balanced by pyridinium cations. A nitrate anion also exists in the outer coordination sphere. As shown in Figure 4, the Th hexanitrato structural units exhibit no significant interactions with the pyridinium cations and thus form an overall 0-dimensional network. By contrast, the outer sphere nitrate anions engage in H-bonding interactions with pyridinium cations (N-H---O distances and angles range from 2.869(4) Å, 148(9)° to 3.056(3) Å, 151(6)°). These interactions together with π-π stacking between pyridinium rings (Cg---Cg distance and angle of 3.5980(25) Å, 22.3°) result in 1-D zig-zag chains that propagate along the [100] (Figure 4).

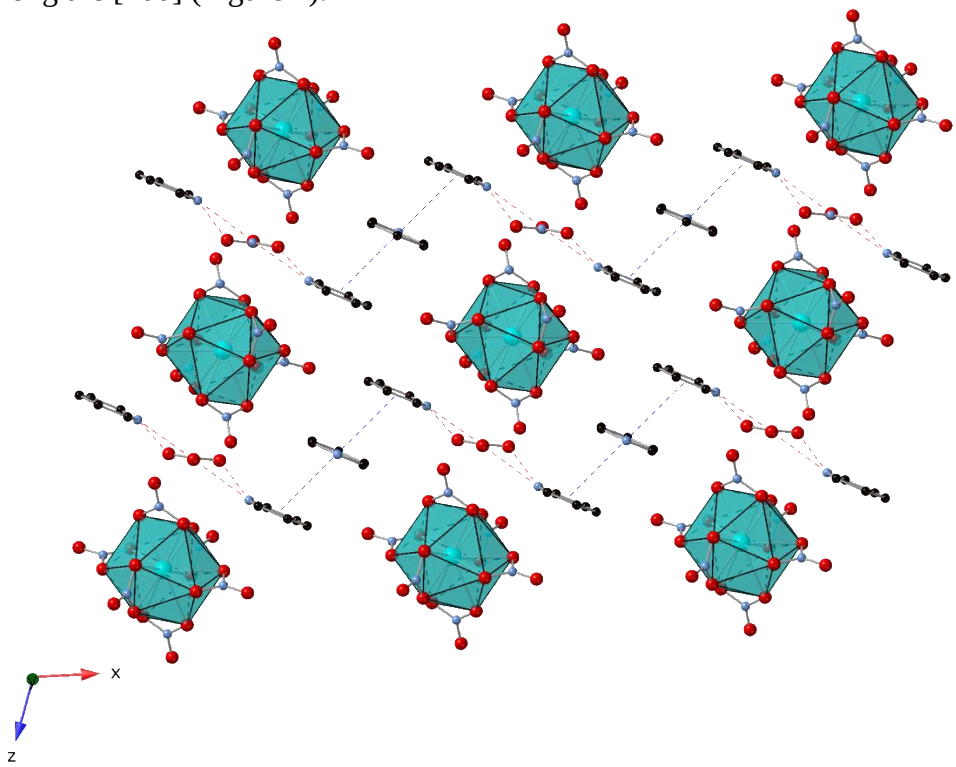

Figure 4. Packing diagram of **3**, $(PyH)_2[Th(NO_3)_6]\bullet(PyH\bullet NO_3)$, showing limited propagation of the Th structural units. By comparison the $[PyH]^{1+}$ and NO_3^{1-} anions form H-bonding interactions (red dashed lines) that together with PyH---PyH π-π stacking interactions (blue dashed lines) yield 1D zig-zag chains. Color code: Th, teal; O, red; N, dark blue; C, black. Hydrogen atoms have been omitted for clarity.

Compound **4**, $(PyH)_2[Th(NO_3)_6]\bullet 2(PyH\bullet NO_3)$, crystallizes in the $P2_1/c$ space group. Like compound **3**, the structure is built from $[Th(NO_3)_6]^{2-}$ anionic units that are charged balanced by pyridinium cations. However, as shown in Figure 5, the nitrate anions of the Th structural units exhibit H-bonding with the pyridinium cations (N-H---O). The pyridinium cations also engage in H-bonding with outer sphere nitrate anions (N-H---O). Nonetheless, propagation of the Th structural units is limited, with the $[Th(NO_3)_6]^{2-}$, pyridinium, and outer sphere nitrate anions forming 0D $(PyH)_2[Th(NO_3)_6]\bullet 2(PyH\bullet NO_3)$ hydrogen bonded units. No significant π-π stacking interactions are observed.

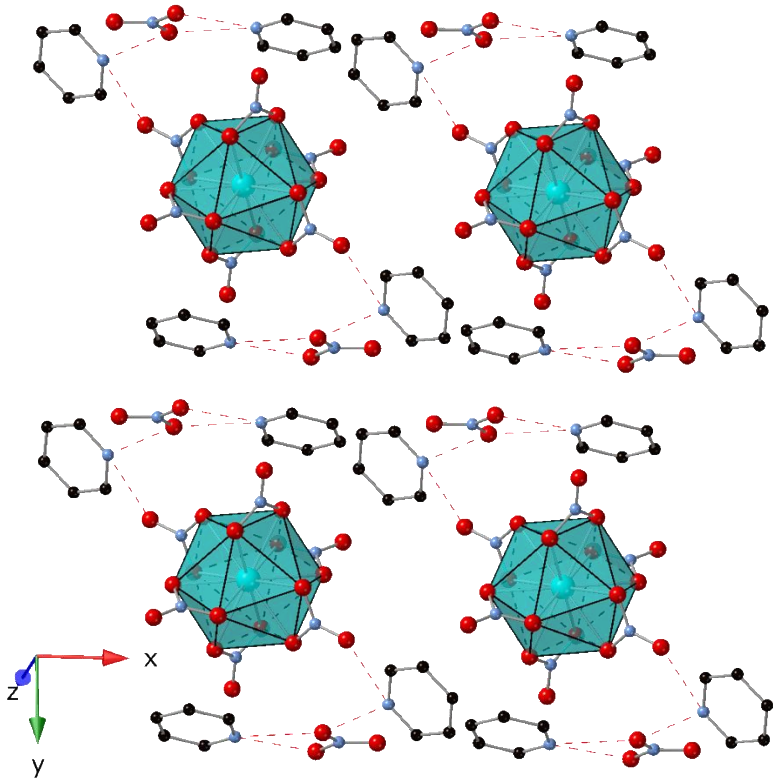

Figure 5. Packing diagram of **4**, $(PyH)_2[Th(NO_3)_6]\bullet 2(PyH\bullet NO_3)$, highlighting the 0D network that is formed through H-bonding (red dashed lines) interactions. Color code: Th, teal; O, red; N, dark blue. Hydrogen and carbon atoms have been omitted for clarity.

Compound **5**, $(3,5\text{-DiMePyH})_2[Th(NO_3)_6]\bullet[(3,5\text{-DiMePyH})(NO_3)]$, crystallizes in the P $2_1/c$ space group. The structure is built from $[Th(NO_3)_6]^{2-}$ anionic units that are charged balanced by 3,5-dimethylpyridinium cations. As shown in Figure 6, the Th structural units form an overall 0-dimensional supramolecular network and exhibit no significant interactions with the outer sphere ions. H-bonding interactions do exist between the outer sphere nitrate anions and 3,5-dimethyl pyridinium cations; the strongest N-H---O interaction distance and angle is 2.965(4) Å and 143(5)°, respectively. Additionally, there exist weak π–π stacking interactions between the 3,5-DiMePyH cations, with a $Cg_{(3,5\text{-DiMePyH})}$---$Cg_{(3,5\text{-DiMePyH})}$ distance of 3.7087(12) Å and slip angle of 23.6°.

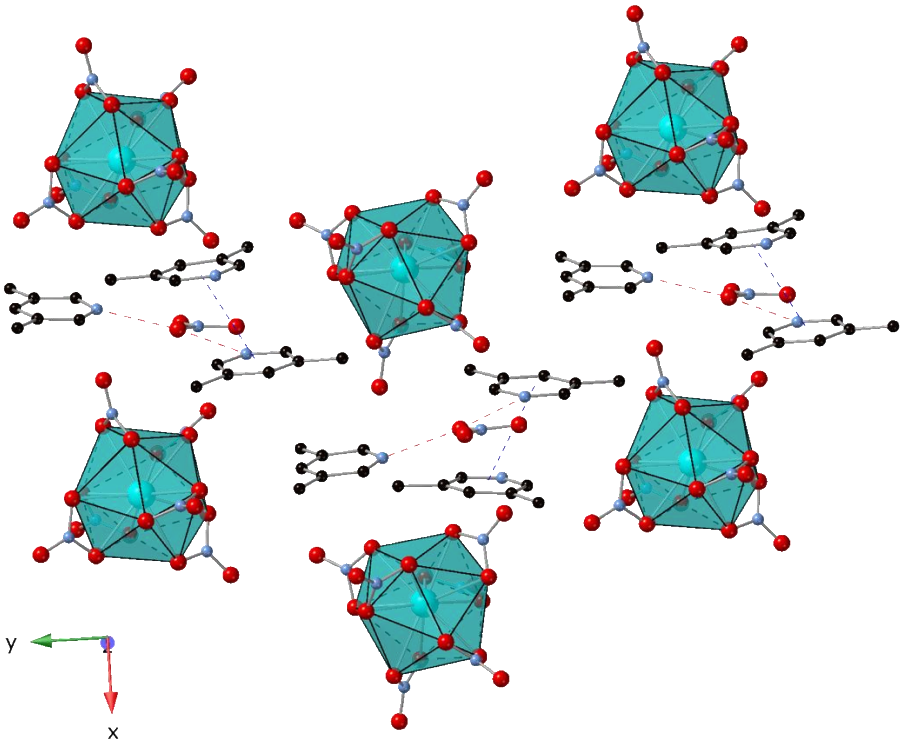

Figure 6. Illustration of the 0D-network of **5**, $(3,5\text{-DiMePyH})_2[Th(NO_3)_6]\bullet[(3,5\text{-DiMePyH})(NO_3)]$,) highlighting the H-bonding (red dashed lines) and π-π stacking (blue dashed lines) between the $[Th(NO_3)_6]^{2-}$ complex and the $[3,5\text{-DiMePyH}]^{1+}$ cations. Color code: Th, teal; O, red; N, dark blue; C, black Hydrogen atoms have been omitted for clarity.

Compound **6**, $(3,5\text{-DiMePyH})_2[Th(NO_3)_6]$, crystallizes in the $P2_1/n$ space group. The structure is built from $[Th(NO_3)_6]^{2-}$ anionic units that are charged balanced by 3,5-dimethylpyridinium cations. As shown in Figure 7, the Th structural units form an overall 0-dimensional supramolecular network, with one of the nitrate anions of the Th complex exhibiting H-bonding interactions with the outer sphere 3,5-dimethyl pyridinium cation. The N-H---O distance and angle is 2.889(3) Å and 154(4) °, respectively. No significant π–π stacking interactions are observed.

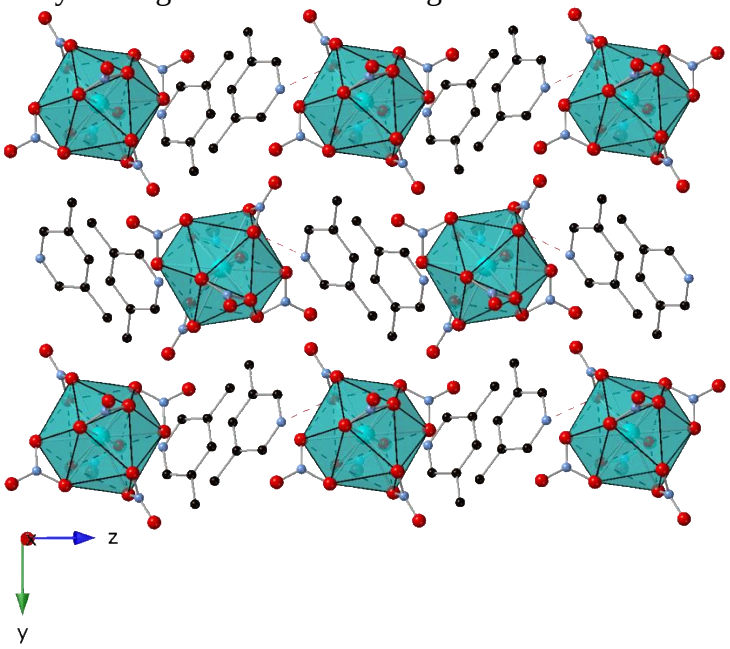

Figure 7. Packing diagram of $(3,5\text{-DiMePyH})_2[Th(NO_3)_6]$ (**6**) highlighting the H-bonding interactions (red dashed lines) between the $[Th(NO_3)_6]^{2-}$ complex and the $[3,5\text{-DiMePyH}]^{1+}$ cations. Overall, the structure adopts a 0D supramolecular network. Color code: Th, teal; O, red; N, dark blue; C, black. Hydrogen atoms have been omitted for clarity.

Compound **7**, $(TerpyH_2)[Th(NO_3)_6]\bullet(TerpyH_2)(NO_3)_2$, crystallizes in the C2/c space group. The structure is built from $[Th(NO_3)_6]^{2-}$ anionic units that are charged balanced by terpyridinium cations. The $[TerpyH_2]^{2+}$ as well as uncoordinated nitrate anions reside in the outer coordination sphere. Little interaction between the Th nitrate complex and the outer sphere ions is observed, with the Th structural units forming a 0-dimensional supramolecular network (Figure 8). Nonetheless, the $[TerpyH_2]^{2+}$ cations engage in N-H---O H-bonding interactions with the free nitrate anions; two unique N-H---O interactions are present with donor-acceptor distances of 2.653(2) and 2.685(2) and N-H---O angles of 166(2)° and 168(2)°, respectively.

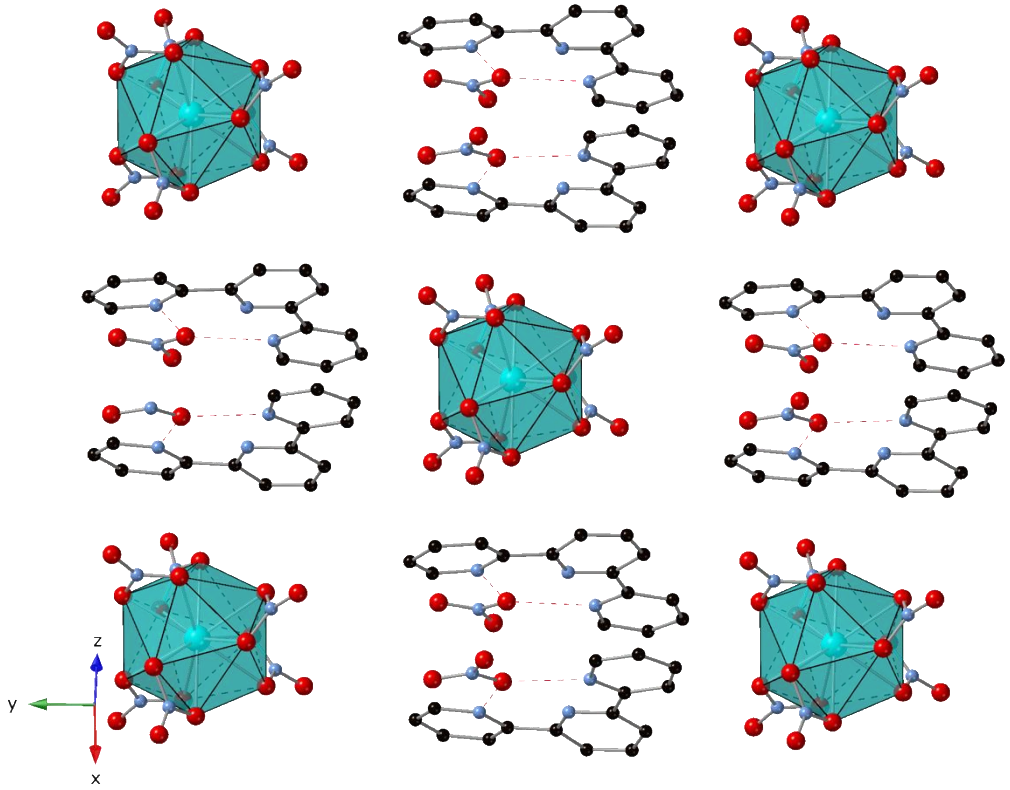

Figure 8. Packing diagram of **7**, $(TerpyH_2)[Th(NO_3)_6]\bullet(TerpyH_2)(NO_3)_2$, showing limited interaction between the Th complexes and the outer sphere $TerpyH_2$ and nitrate ions. N-H---O H-bonding between the $TerpyH_2$ and free nitrate anions is shown as red dashed lines. Color code: Th, teal; O, red; N, dark blue; C, black. Hydrogen atoms have been omitted for clarity.

Compound **8,** $[4\text{-MePyH}]_2[Th(NO_3)_6]$, crystallizes in the $P2_1/n$ space group. The structure is built from $[Th(NO_3)_6]^{2-}$ anionic units that are charged balanced by 4-methylpyridinium cations. As shown in Figure 9, the Th structural units are propagated into 1-dimensional chains via weak H-bonding that exists between the nitrate anions of the $[Th(NO_3)_6]^{2-}$ complexes and the $[4\text{-MePyH}]^{1+}$ cations as well as weak π-π stacking between the $[4\text{-MePyH}]^{1+}$ rings. N-H---O distances and angles range from 2.964(2) Å and 109(2)° to 3.249(2) Å and 159(2)°. π–π stacking interactions exhibit a C_g---C_g distance of 3.791(1) Å and a slip angle of 17.2°.

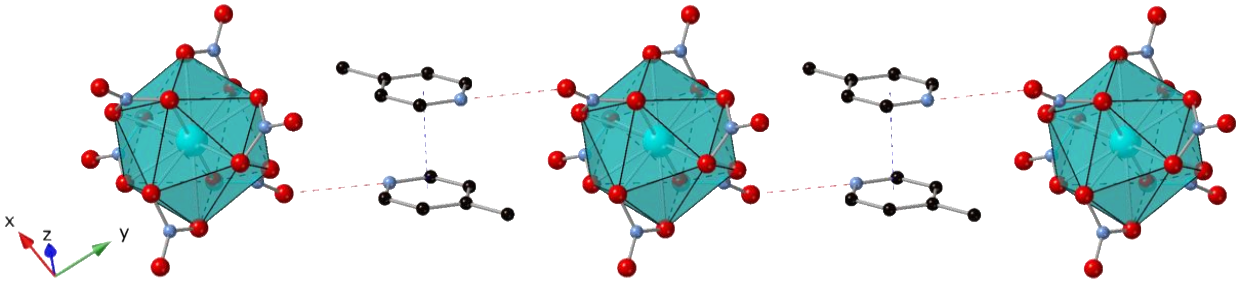

Figure 9. Packing diagram of **8**, $[4\text{-MePyH}]_2[Th(NO_3)_6]$, illustrating the 1D chains that are formed through H-bonding (red dashed lines) and π-π stacking (blue dashed lines) interactions. Color code: Th, teal; O, red; N, dark blue; C, black. Hydrogen atoms have been omitted for clarity.

Compound **9**, $(4,4'\text{-BipyH}_2)_2[\text{Th}(\text{NO}_3)_6]_2\bullet[4,4'\text{-BipyH}_2\bullet 2\text{NO}_3]$, crystallizes in the P-1 space group. The structure is built from $[\text{Th}(\text{NO}_3)_6]^{2-}$ anionic units that are charged balanced by bipyridinium cations. Outer sphere nitrate anions are also present in the structure. As shown in Figure 10, H-bonding interactions between the $[4,4'\text{-BipyH}_2]^{2+}$ cations and the anionic Th complexes (N-H---O distance and angle of 2.762(3) Å, 179(3)°) as well as free nitrate ions (N-H---O distance and angle of 3.038(2), 127(3)°) result in supramolecular 1-dimensional H-bonded chains.

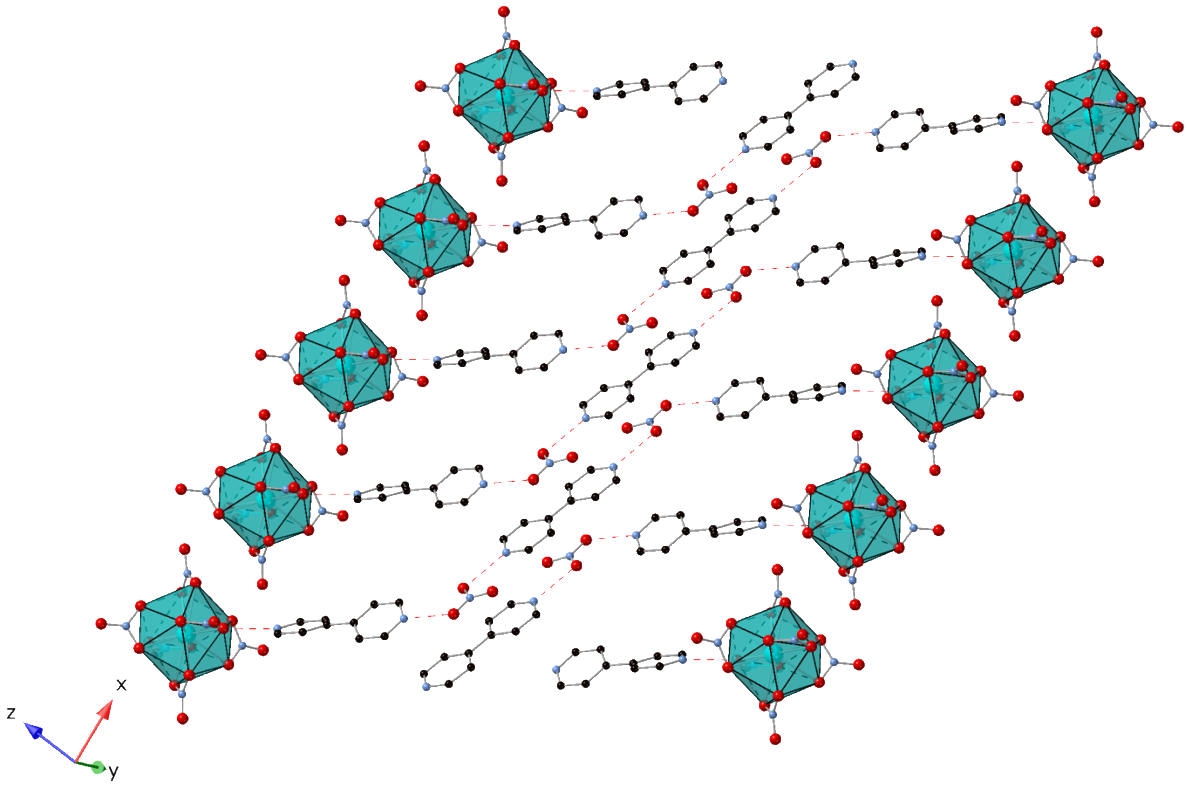

Figure 10. Illustration of **9**, $(4,4'\text{-BipyH}_2)_2[\text{Th}(\text{NO}_3)_6]_2\bullet[4,4'\text{-BipyH}_2\bullet 2\text{NO}_3]$, highlighting the 1D chains that are formed through H-bonding interactions (red dashed lines) between the anionic $\text{Th}(\text{NO}_3)_6^{2-}$ and free NO_3^{1-} units and the $[4,4'\text{-BipyH}_2]^{2+}$ cations. Color code: Th, teal; O, red; N, dark blue; C, black. Hydrogen atoms have been omitted for clarity.

Compound **10**, $(PhthalH)_2[Th(NO_3)_6]$, crystallizes in the C2/c space group. The structure is built from $[Th(NO_3)_6]^{2-}$ units that are charged balanced by phthalazinium cations. As shown in Figure 11, H-bonding between the anionic Th complexes and the cationic $[PhthalH]^{1+}$ as well as $Cg_{(PhthalH)}$---$Cg_{(PhthalH)}$ π–π stacking interactions result in 1-dimensional zig-zag chains that propagate along the [100]. The N-H---O interaction distance and angle is 2.968(5) Å and 158(2)° and the $Cg_{(PhthalH)}$--- $Cg_{(PhthalH)}$ distance and slip angle are 3.629(2) Å and 21.5°, respectively.

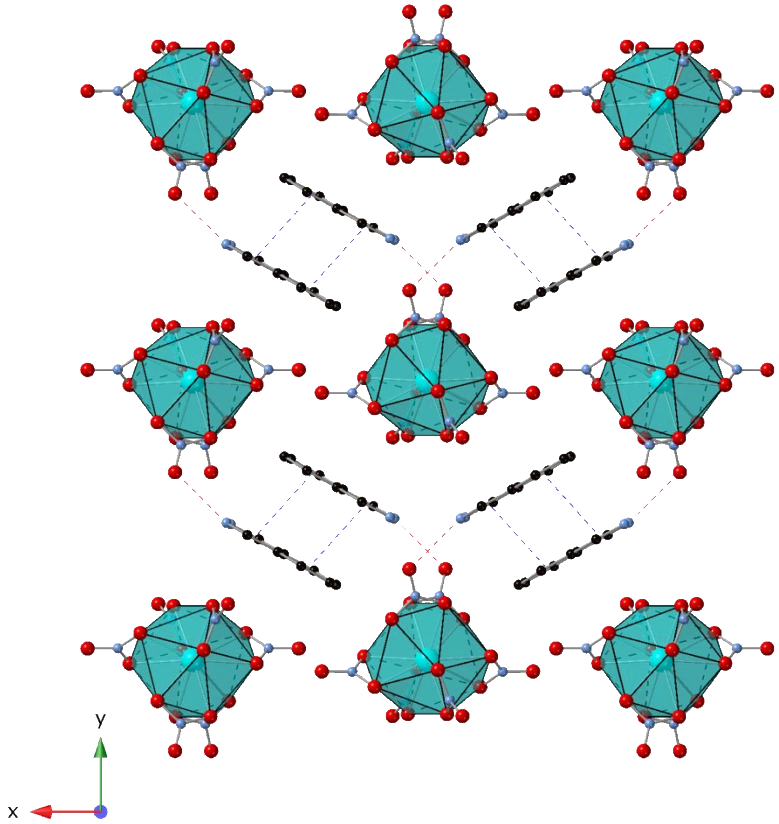

Figure 11. Packing diagram of **10**, $(PhthalH)_2[Th(NO_3)_6]$, highlighting the 1D chains that are formed via H-bonding (red dashed lines) and π-π stacking interactions (blue dashed lines). Color code: Th, teal; O, red; N, dark blue; C, black. Hydrogen atoms have been omitted for clarity.

Compound **11**, $(TerpyH_2)[Th(NO_3)_6]\bullet[H_2O]$, crystallizes in the $P2_1/n$ space group. The structure is built from $[Th(NO_3)_6]^{2-}$ anionic units that are charged balanced by terpyridinium cations. Free water molecules also exist in the outer coordination sphere. The nitrate anions of the $[Th(NO_3)_6]^{2-}$ complexes participate in hydrogen bonding with unbound water molecules. These $O_{(NO3)}$-H---$O_{(H2O)}$ H-bonding interactions link the Th structural units along the [100] into 1-dimensional chains as shown in Figure 12, with a donor-acceptor distance and angle of 2.771(2) Å and 177(2)°, respectively. The outer sphere water molecules also interact with the $TerpyH_2$ cations with a N-H---O interaction distance and angle of 2.745(3) Å and 155(3)°, respectively. In addition to H-bonding, the $[TerpyH_2]^{2+}$ exhibit weak π-π stacking interactions ($C_{(TerpyH2)}$---$C_{(TerpyH2)}$ distance of 3.777(12) Å and slip angle of 24.4°). Taken together, the H-bonding between the Th complexes, water molecules, and $TerpyH_2$ and the π–π stacking interactions result in "thick" 1-dimensional chains.

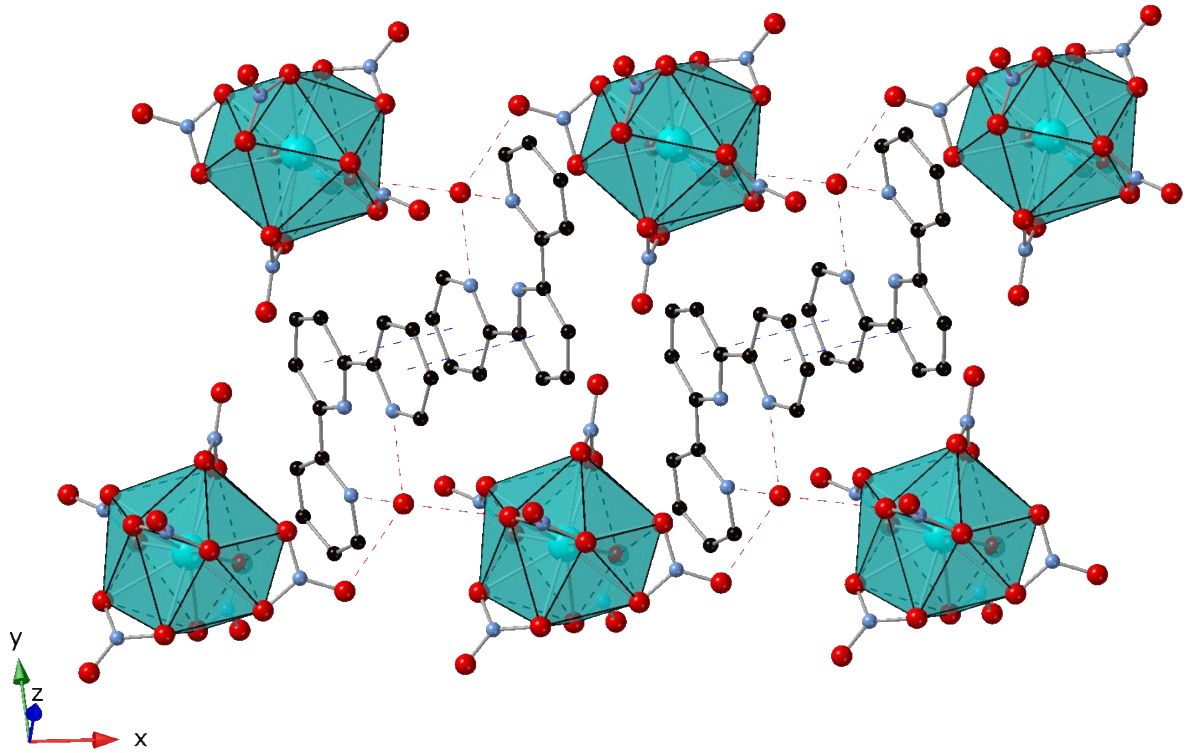

Figure 12. Illustration of $(TerpyH_2)[Th(NO_3)_6]\bullet[H_2O]$, (**11**) highlighting the "thick" 1D chains that are formed through H-bonding (red dashed lines) and π-π stacking interactions (blue dashed lines). Color code: Th, teal; O, red; N, dark blue; C, black. Hydrogen atoms have been omitted for clarity.

Compound **12**, $(2\text{-MePyH})_2[Th(NO_3)_6]\bullet 2H_2O$, crystallizes in the C2/c space group. The structure is built from $[Th(NO_3)_6]^{2-}$ anionic units that are charged balanced by 2-methyl pyridinium cations. Free water molecules also exist in the outer coordination sphere. Overall, the structure adopts a 2-dimensional supramolecular network that is characterized by O-H---O H-bonding interactions (Figure 13a) that exist between the nitrates from the Th complex and outer sphere water molecules. A representative O-H---O interaction distance and angle is 2.887(2) Å and 168(3)°. As shown in Figure 13b, the $[2\text{-MePyH}]^{1+}$ cations only engage in H-bonding with the free water molecules, with a N-H---O interaction distance and angle of 2.711(3) Å and 169(3)°, respectively. Yet these interactions are isolated and do not extend the connectivity of the network.

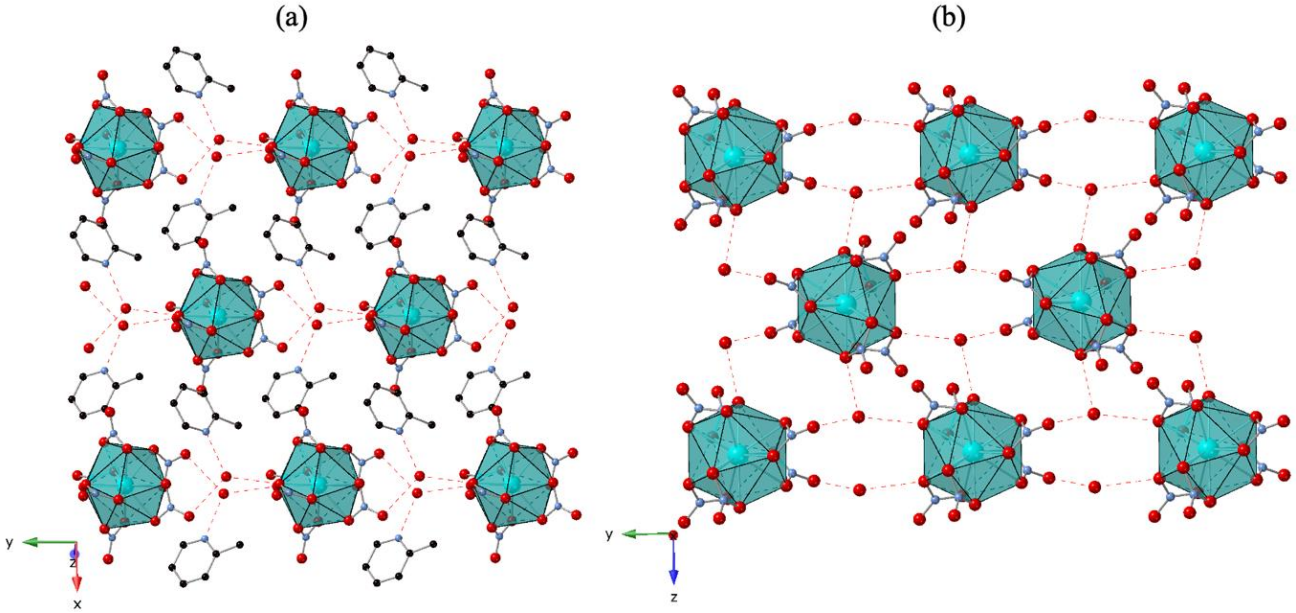

Figure 13. Illustration of $(2\text{-MePyH})_2[Th(NO_3)_6]\bullet 2H_2O$ (**12**) highlighting (a) the 2D sheets that are formed through H-bonding interactions (red dashed lines) and (b) the H-bonding interactions between the 2-MePyH and water molecules. Color code: Th, teal; O, red; N, dark blue; C, black. Hydrogen atoms have been omitted for clarity.

Compound **13**, $(3\text{-MePyH})_2[Th(NO_3)_6]$, crystallizes in the C2/c space group. The structure is built from $[Th(NO_3)_6]^{2-}$ anionic units that are charged balanced by 3-methylpyridinium cations. Overall, the structure adopts a 2-dimensional supramolecular network that is formed by H-bonding and π–π stacking interactions. As shown in Figure 14, the 3-MePyH cations engage in H-bonding with the nitrate oxygen atoms of the $[Th(NO_3)_6]^{2-}$ complexes with donor-acceptor distances of 2.833(4) Å and 3.093(4) Å and N-H---O angles of 143(4)° and 127(4)°, respectively. These interactions together with strong π–π stacking interactions between the $[3\text{-MePyH}]^{1+}$ cations ($Cg_{(3\text{-MePyH})}$---$Cg_{(3\text{-MePyH})}$ distance and slip angle of 3.572(2) Å and 7°, respectively) result in sheets that extend along the [001] and [100].

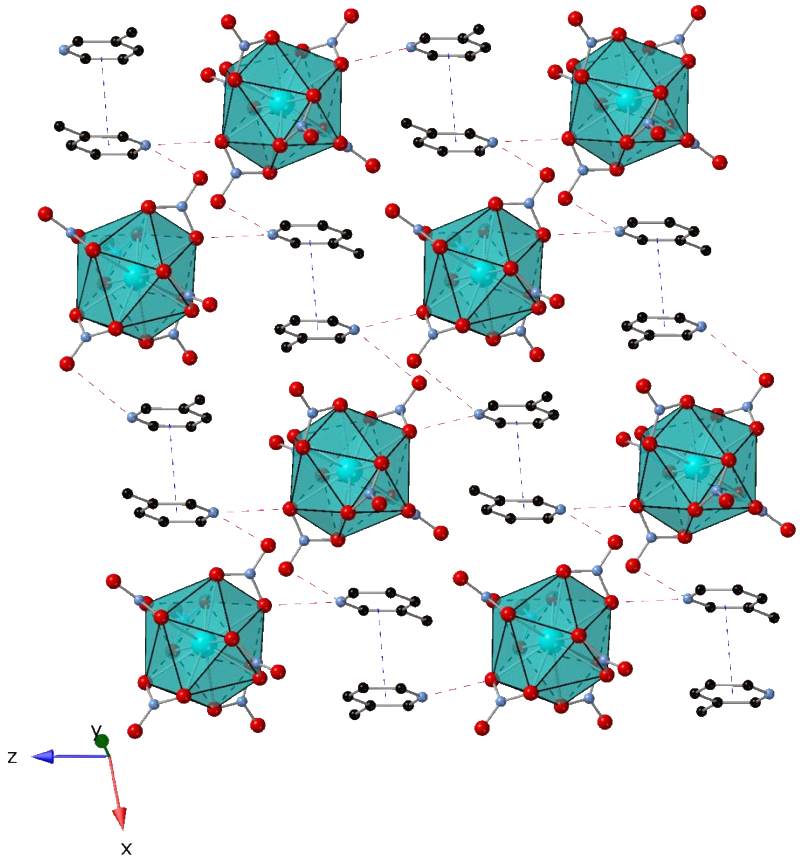

Figure 14. Packing diagram of **13**, $(3\text{-MePyH})_2[Th(NO_3)_6]$, highlighting the 2D sheets that are formed through H-bonding (red dashed lines) and π-π stacking interactions (blue dashed lines). Color code: Th, teal; O, red; N, dark blue; C, black. Hydrogen atoms have been omitted for clarity.

Compound **14**, $(3\text{-ClPyH})_2[Th(NO_3)_6]$, crystallizes in the C2/c space group. The structure is built from $[Th(NO_3)_6]^{2-}$ anionic units that are charged balanced by 3-chloropyridinium cations. The structure is isomorphous with **13** and adopts a 2-dimensional network characterized by H-bonding and π–π stacking interactions. The donor-acceptor distances for the $[3\text{-ClPyH}]^{1+}$---$(NO_3)^{1-}$ N-H---O interactions are 2.79(3) Å and 3.06(3) Å with angles of 155(3)° and 119(2)°, respectively. The $Cg_{(3\text{-ClPyH})}$ ---$Cg_{(3\text{-ClPyH})}$ distance is 3.56(2) Å and has a slip angle of 8.1°.

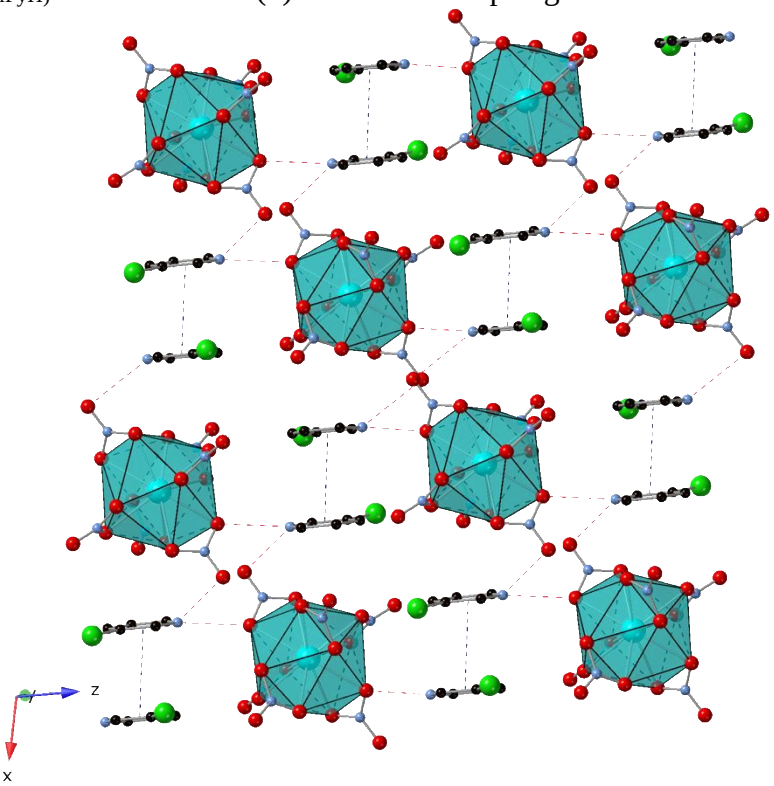

Figure 15. Packing diagram of **14**, $(3\text{-ClPyH})_2[Th(NO_3)_6]$, highlighting the 2D sheets that are formed through H-bonding (red dashed lines) and π-π stacking interactions (blue dashed lines) between Th structural units. Color code: Th, teal; O, red; Cl, green; N, dark blue; C, black. Hydrogen atoms have been omitted for clarity.

Compound **15**, $(PhenH)_2[Th(NO_3)_6]\bullet 2[H_2O]$, crystallizes in the $P2_1/n$ space group. The structure is built from $[Th(NO_3)_6]^{2-}$ anionic units that are charged balanced by phenanthrolinium cations. Free water molecules also exist in the outer coordination sphere. Overall, the structure adopts a 2-dimensional supramolecular network consisting of H-bonding interactions (Figure 16) between the Th nitrate complex, the outer sphere water molecules, and the $PhenH^{1+}$. The nitrates of the $[Th(NO_3)_6]^{2-}$ unit interact with outer sphere water molecules with the strongest O-H---O interaction exhibiting a distance and angle of 2.924(2) Å and 165(3)°, respectively. The water molecules further engage with the N-H of $PhenH^{1+}$ with an N-H---O interaction distance and angle of 2.735(3) Å and 157(3)°. Additionally, the phenanthrolinium cations exhibit offset π-π stacking interactions along the [100] with a $C_{(PhenH)}$---$C_{(PhenH)}$ distance of 3.7087(12)Å and a slip angle of 23.6(7)°.

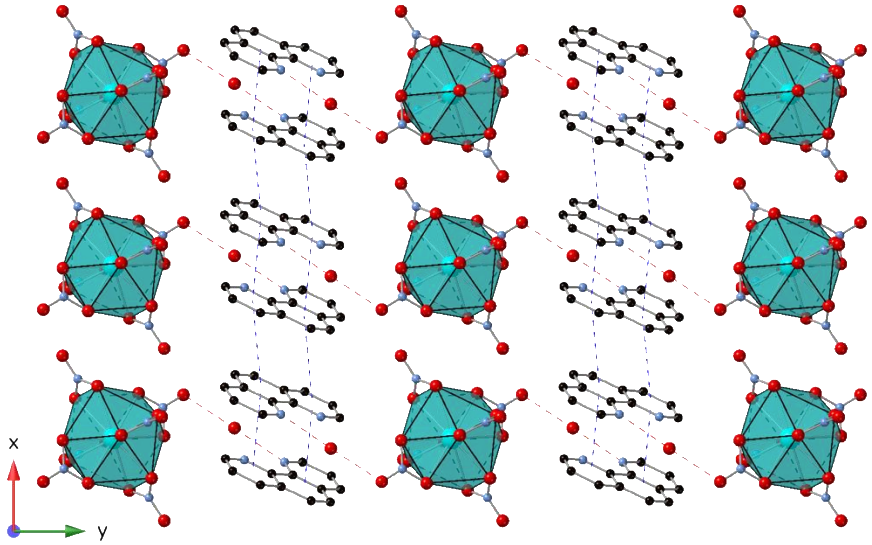

Figure 16. Packing diagram of **15**, $(PhenH)_2[Th(NO_3)_6]\bullet 2[H_2O]$, highlighting the 2D sheets that are formed through H-bonding (red dashed lines) and π-π stacking interactions (blue dashed lines). Color code: Th, teal; O, red; N, dark blue; C, black. Hydrogen atoms have been omitted for clarity.

Relationship to other previously reported Th-nitrate complexes.

Solution state studies have been foundational to our understanding of actinide speciation.[60] However, for ions such as Th^{4+} that are highly charged and highly hydrolysable, with low solubility products, solid-state structural chemistry has provided a valuable, complementary approach for understanding actinide coordination chemistry.[15] As such, in this work we employ edsolid-state and in silico data to further understand thorium nitrate speciation. Fifteen Th-nitrate compounds were isolated yet Th^{4+} adopted only two unique structural units in nitrate ligand systems in the presence of various protonated N-heterocycles capable of H-bond donation. This limited structural chemistry (in terms of the metal complex speciation) is in stark contrast to our group's previous work in chloride ligand systems that yielded five distinct structural units,[27] ranging from chloride deficient to chloride rich complexes. As previously described, thorium chloride bonding interactions are generally considered weak.[61] We proposed that this feature lent Th-Cl complexation to greater variability in metal-complexation and that weak noncovalent interactions could thereby serve to stabilize various structural units. While nitrate is similar to chloride in that both ligands are monoanionic and known to form relatively weak complexes,[3] nitrate differs from chloride as NO_3^{1-} anions tend to coordinate tetravalent metal cations solely in a bidentate fashion.[62] Chloride is generally monodentate[18] although it can serve to bridge multiple metal centers.[30] In fact, recent work showing that the free energies of formation of $[Th(NO_3)_n]$ complexes are slightly larger than seen for other monovalent ions, including chloride, likely reflects the bidentate nature of nitrate;[18] both anion charge and coordination mode are important for assessing the strength of the complex formed.

Looking to the literature, our observation of limited metal-complex speciation is consistent with other work in thorium nitrate systems.[63] In the absence of counterions, early work by Ferraro et al suggested that at 25 °C the only two relevant (precipitating) solids were $Th(NO_3)_4(H_2O)_4$ and $Th(NO_3)_4(H_2O)_5$.[64] Later work by Soderholm et al, showed that in solution the Th solution speciation saturates at $[Th(NO_3)_3]^{1+}$.[15] Two phases were isolated from these solutions – $Th(NO_3)_4(H_2O)_4$ and $Th(NO_3)_4(H_2O)_3 \bullet 2(H_2O)$. The absence of anionic units is attributed to the absence of counterions in solution. By comparison, in the presence of alkali metal and tetraalkylammonium cations, Th solid-state structural chemistry is dominated by the formation of the hexanitrato phase.[65] However, limited examples of the pentanitrato complex have also been reported, with cation hydration enthalpy having been found to drive the stabilization of one unit over the other. In the current work, we likewise see the formation of only the pentanitrato and hexanitrato structural units in the solid-state. Importantly, our results show that cations drive the precipitation of anionic Th-nitrate complexes and highlight a clear favorability of the Th-hexanitrato molecular unit.

Predicted Displacement Reaction Energies

Building on the approaches used to study Th-Cl and Th-Br systems,[28,66] electronic structure calculations at the density functional theory and correlated molecular orbital theory levels were used to predict the relative energetics between a range of Th^{IV}–aquo–nitrate complexes. The lowest energy structures for different species were predicted as a function of the number of ligands in the

first coordination shell (Table 3). The geometries were optimized at the DFT/B3LYP level in aqueous solution to prevent loss of water molecules from the first solvation shell. The best values are given by the CCSD(T) values using the aqueous optimized geometry, and these are the values discussed herein.

We have previously shown that the most stable isolated Th^{IV} species is $Th(H_2O)_9^{4+}$ if no counterion ligands are included in the solution.[27] Table 3 gives the most stable species for each number of nitrate ligands bonded to the Th^{4+} in aqueous solution. With one nitrate, the structure with 8 H_2O molecules is more stable than one with 7 H_2O molecules and the nitrate is monodentate giving a coordination number of 9 for the former. With 2 nitrate ligands, the structure with 7 H_2O molecules is more stable than one with 6 H_2O molecules. For the most stable structure, there are one bidentate and one monodentate ligand giving a coordination number of 10. When 3 nitrates are present, the hexa-aquo complex is preferred with 2 monodentate and one bidentate giving a coordination number of 10. With 4 nitrate groups, the structure with 5 H_2O molecules is the most stable with the nitrates all monodentate giving a coordination number of 9. With 5 nitrates, the structure with two water molecules is more stable than one with 3 water molecules. In the lowest energy structure of $Th(H_2O)_2(NO_3)_5^{1-}$, there are 5 bidentate nitrates and two H_2O molecules giving a coordination number of 12, just as found in the solid state. The corresponding structure with 3 bidentate ligands, two monodentate ligands and two H_2O molecules for a coordination number of 10 is 11.6 kcal/mol higher in energy. For the hexanitrato dianion, the most stable structure is the one with 6 bidentate nitrates giving a coordination number of 12, again as found in the solid state. The structure with one H_2O molecule in the inner coordination sphere with 5 bidentate and one monodentate ligands giving a coordination number of 12 is 6.9 kcal/mol higher in energy. The $Th(NO_3)_6^{2-}$ structure with 4 bidentate ligands and two monodentate ligands for a coordination number of 10 is 15.8 kcal/mol higher in energy. The $Th(H_2O)_2(NO_3)_5^{1-}$ structure with 4 bidentate ligands, two monodentate ligands, and a H_2O molecule with a coordination number of 11 is 21.3 kcal/mol higher in energy than the most stable hexanitrate structure. As nitrate ligands are added, the coordination number increases up to 12 except for the neutral nitrate where the coordination number reverts back to 9.

Table 3. Calculated Reaction Energies, ΔG_{aq}, for thorium(IV)-nitrate structures at 298 K with the aD basis set.[a]

Reaction	B3LYP	MP2	CCSD(T)
$Th(H_2O)_8NO_3^{3+} \rightarrow Th(H_2O)_7NO_3^{3+} + H_2O$	2.7	9.7	9.8
$Th(H_2O)_7(NO_3)_2^{2+} \rightarrow Th(H_2O)_6(NO_3)_2^{2+} + H_2O$	-0.6	6.5	6.4
$Th(H_2O)_6(NO_3)_3^{1+} \rightarrow Th(H_2O)_5(NO_3)_3^{1+} + H_2O$	-3.8	3.3	3.4
$Th(H_2O)_5(NO_3)_4 \rightarrow Th(H_2O)_4(NO_3)_4 + H_2O$	-3.6	5.6	6.5
$Th(H_2O)_3(NO_3)_5^{1-} \rightarrow Th(H_2O)_2(NO_3)_5^{1-} + H_2O$	-7.4	-16.8	-16.7
$Th(H_2O)(NO_3)_6^{2-} \rightarrow Th(NO_3)_6^{2-} + H_2O$	-9.5	-7.0	-6.9

[a] Optimized at the B3LYP/DZVP2/COSMO(aq) level.

The energetics for the stepwise addition of nitrate to $[Th(H_2O)_9]^{4+}$ to ultimately form the hexanitrato are shown in Table 4. Addition of nitrate to the hydrated Th^{IV} with H_2O displacement is slightly exothermic by *ca*. -1 kcal/mol. The substitution of the second nitrate with H_2O displacement is more exothermic by *ca*. -12 kcal/mol. Substitution of the third nitrate for H_2O is slightly exothermic by *ca*. -2 kcal/mol. Displacement of the H_2O by a fourth nitrate to generate the neutral cluster is now endothermic by *ca*. 4 kcal/mol. The next displacement reaction by nitrate

eliminates 3 H_2O molecules and is highly exothermic by ca. -26 kcal/mol. The displacement of H_2O from $Th(H_2O)_2(NO_3)_5^{1-}$ by nitrate to form $Th(H_2O)(NO_3)_6^{2-}$ is slightly endothermic by *ca*. 4 kcal/mol. The loss of 2 H_2O from $Th(H_2O)_2(NO_3)_5^{2-}$ accompanied by substitution of NO_3^{1-} is slightly exothermic by ca. -3 kcal/mol. Overall, the sum of the reactions to generate $Th(NO_3)_6^{2-}$ starting from $Th(H_2O)_9^{4+}$ is exothermic and there are clear sinks at $Th(H_2O)_2(NO_3)_5^{1-}$ and $Th(NO_3)_6^{2-}$.

Thus, the calculated energetic results are consistent with formation of the pentanitrato and hexanitrato species observed experimentally. The nitrates will displace H_2O molecules with thermodynamic sinks at $Th(H_2O)_2(NO_3)_5^{1-}$ and $Th(NO_3)_6^{2-}$. This analysis does not consider the presence of the counter cations that are present and the associated K_{sp}. It is somewhat surprising that the neutral $Th(H_2O)_5(NO_3)_4$ does not precipitate as it does for the tetra-bromide, but it could be that the presence of a highly exothermic step forming the penta-nitrate prevents any type of equilibrium from being established leading to a lack of precipitation of the neutral. In addition, the presence of the templating cations will not favor precipitation of the neutral or cationic nitrates.

Table 4. Calculated reaction energies, ΔG_{aq}, for the stepwise addition of nitrate to 9-coordinate thorium(IV)-nitrate complexes with the aD basis set[a]

Reaction	B3LYP	MP2	CCSD(T)
$Th(H_2O)_9^{4+} + NO_3^{1-} \rightarrow Th(H_2O)_8NO_3^{3+} + H_2O$	0.3	-0.6	-1.8
$Th(H_2O)_8NO_3^{3+} + NO_3^{1-} \rightarrow Th(H_2O)_7(NO_3)_2^{2+} + H_2O$	-2.5	-11.2	-12.2
$Th(H_2O)_7(NO_3)_2^{2+} + NO_3^{1-} \rightarrow Th(H_2O)_6(NO_3)_3^{1+} + H_2O$	2.3	-1.2	-1.7
$Th(H_2O)_6(NO_3)_3^{1+} + NO_3^{1-} \rightarrow Th(H_2O)_5(NO_3)_4 + H_2O$	4.8	4.2	3.6
$Th(H_2O)_5(NO_3)_4 + NO_3^{1-} \rightarrow Th(H_2O)_2(NO_3)_5^{1-} + 3H_2O$	-12.7	-26.3	-26.2
$Th(H_2O)_2(NO_3)_5^{1-} + NO_3^{1-} \rightarrow Th(H_2O)(NO_3)_6^{2-} + H_2O$	5.8	3.2	3.6
$Th(H_2O)_2(NO_3)_5^{1-} + NO_3^{1-} \rightarrow Th(NO_3)_6^{2-} + 2H_2O$	-3.8	-3.8	-3.3

[a] Optimized at the B3LYP/aD/COSMO(aq) level

Vibrational Spectroscopy

For metal ions with no f-electrons, such as Th, vibrational spectroscopy has proven a valuable tool for further examining actinide-ligand bonding as well as the relative strength of noncovalent interactions.[10,67–70] As such, compounds **1-15** were examined using Raman and IR spectroscopy; the spectra for **14**, $[3\text{-ClPyH}]_2[Th(NO_3)_6]$, are presented in Figure 17 as a representative example and the spectra for the other compounds are provided as Supplementary Information (Figures S46-S60).

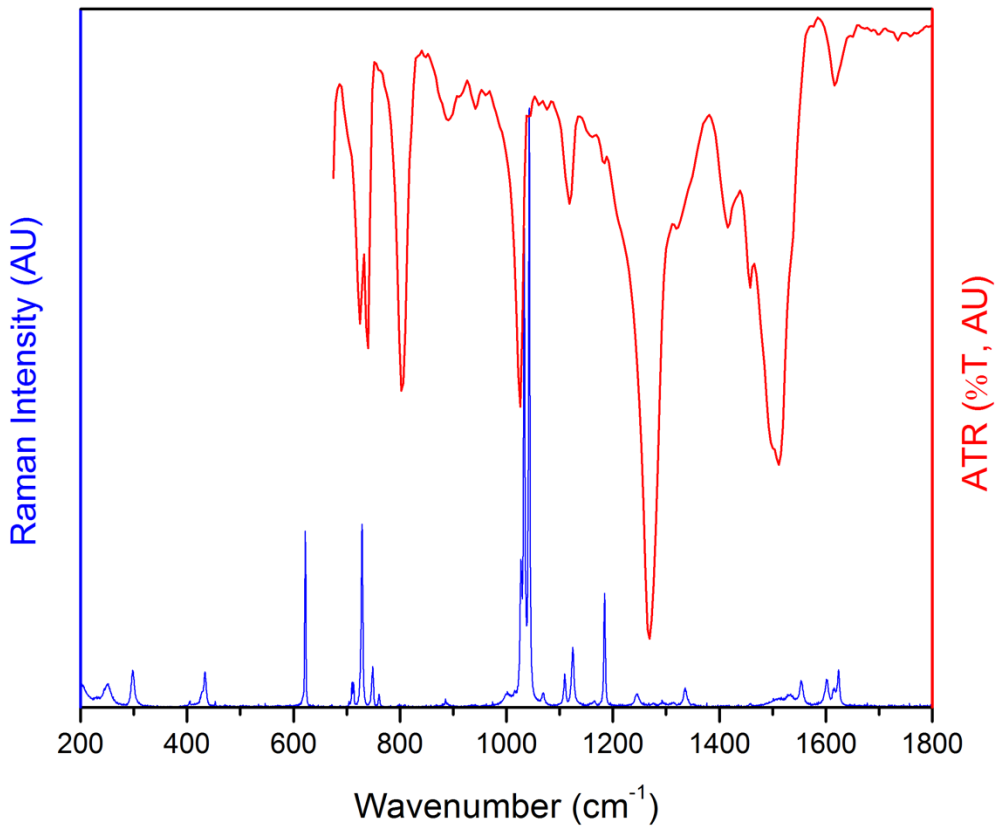

Figure 17. Infrared (IR) and Raman spectra of **14** plotted over 200–1800 cm^{-1} (Raman = blue, IR = red).

As highlighted in Figure 17, both the Raman and IR spectra for **1-15** are dominated by vibrations consistent with the outer coordination sphere NH-heterocycle, and the nitrate ions. Unsurprisingly, across the fifteen compounds, the most significant differences in the Raman and IR spectra of **1-15** arise from changes in the identity of the organic cation present in the structures. The vibrations attributed to C-N and C-C bonds, present in each of the N-heterocycles, are typically observed over 1000-1750 cm^{-1} in the Raman spectra and over around 700-1600 cm^{-1} in the IR.[27,67] For **14**, peaks at 1,128 cm^{-1}, 1,597 cm^{-1}, and 1624 cm^{-1} are thus in good agreement with C-H, C-C, and C-N stretches of the $[3\text{-ClPyH}]^{1+}$.[71] Due to the overlapping nature of the vibrational modes, no factor group splittings were resolved

Examination of the vibrations associated with the independent $Th(H_2O)_2(NO_3)_5^{1-}$ and $Th(NO_3)_6^{2-}$ structural units can be analyzed in terms of the motions of the ligand groups, NO_3^- and H_2O. Electronic structure calculations facilitated identification of these modes; the predicted and observed Raman and IR frequencies as well as assignments are provided in Tables S1-S2. We first describe the results for the hexanitrato dianion, $Th(NO_3)_6^{2-}$. The N-O terminal stretch of the nitrate group is predicted to have significant IR intensity with moderate Raman intensity over 1550 to 1490 cm^{-1}. For **14**, the N-O stretch is observed experimentally with strong IR intensity at 1,551 cm^{-1} and relatively weak Raman intensity at 1552 cm^{-1}. The asymmetric NO_2 group stretch of the nitrates is predicted to have significant IR intensity but only weak Raman intensity around 1300 cm^{-1}. Based on this, the experimentally observed peak at 1273 cm^{-1} with strong IR intensity, and the band at 1336 cm^{-1} with weaker Raman intensity are assigned to this mode. Calculated stretches

from 1000 to 1050 cm^{-1} are consistent with the symmetric NO_2 stretch, with the transition at ~ 1060 cm^{-1} exhibiting a large Raman intensity and the transition at ~ 1020 cm^{-1} having significant IR intensity. The experimentally observed bands over 1016-1033 cm^{-1} in the Raman spectrum and the intense peak at 1026 cm^{-1} in the IR are consistent with these predicted values. For the lower frequency bands, the IR and Raman intensities significantly decrease. The six predicted transitions near 790 cm^{-1} arise from inversions of the NO_3^{1-} group and the six transitions from 750 to 715 cm^{-1} are the symmetric ONO bends of the NO_2 groups. Experimentally these modes are observed at a higher Raman frequency, with peaks at 728, 741, and 769 cm^{-1}. Six transitions are predicted between 695 to 670 cm^{-1} and arise from terminal NO_2 bends; the band at 622 cm^{-1} in the Raman spectra of **14** is consistent with this assignment. There is a significant break until near 200 cm^{-1}, where the predicted bands are the stretches of the NO_3^{1-} ligands with respect to the Th^{4+}. These NO_3^{1-} group stretches and rocks extend down to 165 cm^{-1} and the remaining modes are again attributed to interactions of the nitrate ligands with the Th in terms of rocks, bends, etc. We tentatively assign peaks observed in the experimental Raman spectrum over 219-240 cm^{-1} and at 242 cm^{-1} to these modes. Unfortunately, range limitations of our instrumentation precluded observation of these modes in the IR spectrum.

By comparison the Th dihydrate pentanitrato unit, $Th(H_2O)_2(NO_3)_5^{1-}$, has two approximately equivalent axial H_2O molecules and five approximately equivalent bidentate nitrates. An example of this structural unit is observed in **1**; the IR and Raman spectra are provided in Figure S46. The results follow a similar pattern as that predicted and observed for $Th(NO_3)_6^{2-}$. Unlike the hexanitrato unit, however, for the pentanitrato unit, there are also two predicted sets of H_2O rocks at ~ 560 and ~ 340 cm^{-1} with significant IR intensity, and the H_2O-Th^{4+} stretches at 284 and 256 cm^{-1} with moderate IR intensity. However, as already noted, due to range limitations of the IR microscope, these stretches cannot be observed experimentally. The predicted stretches below 250 cm^{-1} are the coupled NO_3^{1-} group and H_2O group transitions relative to the central Th^{4+}. The calculated modes near 3800 cm^{-1} are due to the H_2O O-H asymmetric and symmetric stretches; these modes were not observed experimentally. There are two predicted H_2O bends near 1625 cm^{-1} with significant IR intensity, this stretch is observed in the IR spectrum of **1** at 1624 cm^{-1}. Five unique NO nitrate stretches are calculated from 1550 cm^{-1} to 1500 cm^{-1} and can mix with the H_2O bends. Two of the transitions have very large IR intensities. A peak at 1520 cm^{-1} is observed experimentally in the IR spectrum of **1** it exhibits very weak IR intensity. The predicted NO_2 group asymmetric stretches range from 1310 to 1285 cm^{-1} and the highest frequency transition has a large IR intensity. This stretch is observed experimentally with significant IR intensity at 1318 cm^{-1}. There are five predicted NO_2 symmetric stretches near 1060 cm^{-1} with only moderate IR intensity. For **1** this peak is observed experimentally at 1045 cm^{-1} and is in good agreement with the calculated value. There are five calculated transitions near 790 cm^{-1} due to NO_3^{1-} group inversions at N. The five calculated NO_2 bends are from 750 to 730 cm^{-1} and the five O-NO_2 bends are predicted at approximately ~ 690 cm^{-1}; for **1** these modes are not observed experimentally. Collectively, these results point to relatively few, but discernable features (e.g. H_2O bends) that could be used to differentiate the thorium-nitrato structural units.

Electrostatic Potential Surfaces.

The ability of noncovalent interactions to influence speciation of actinides ions in solution and the solid state continues to drive investigations into different Th systems. The thorium(IV) nitrate species reported herein show a remarkable resistance to speciation in the presence of different

organic cations. As already noted, this is in contrast to our past studies of thorium(IV) aqua-chloro systems showing eight different $[Th(H_2O)_xCl_y]$ units when paired with as many organic cations. Here, only the $[Th(NO_3)_6]^{2-}$ and $[Th(H_2O)_2(NO_3)_5]^{1-}$ are observed experimentally, of which the hexanitrato species dominates. To probe this, we examined the ESP surfaces of these species (Figure 18; Table 5). The $[Th(NO_3)_6]^{2-}$ species has an overall charge of -2 making all potential values negative and therefore electron rich. Of these, the coordinated O atoms have the lowest potential values owing to polarization about the coordinated nitrate ligand. These atoms are thus the most electron rich areas whereas the uncoordinated O atom, by comparison, has the lowest electron density. The modest -1 charge of the $[Th(H_2O)_2(NO_3)_5]^{1-}$ unit gives rise to regions of both positive and negative potential values. The coordinated water molecules are polarized along the O-H bond leaving electron depletion at the H atoms and positive potential values (63 kJ/mol) which may serve as hydrogen bond donors. Negative potential values and electron rich areas are located at the coordinated nitrate ligands. The spatial distribution of the coordinated nitrate and water ligands results in a dramatically different landscape for the two Th units found in **1-15**. The hexanitrato unit is strictly electron rich where the electron density is fairly evenly distributed about the surface as indicated by the difference of the maximum (-527 kJ/mol) and minimum ESP values (-607 kJ/mol) at 80 kJ/mol (ΔE). The delocalized electron distribution limits $[Th(NO_3)_6]^{2-}$ to act as a hydrogen bond acceptor. Such is not the case with the aqua-pentanitrato unit, which has a large ΔE value of 385 kJ/mol and electron density localized to the equatorial plane perpendicular to the H_2O-Th-OH_2 bonding axis. As such, the $[Th(H_2O)_2(NO_3)_5]^{1-}$ is capable of forming noncovalent hydrogen bonding interactions as both a bond donor *and* acceptor, both of which are observed experimentally between Th units and organic cations.

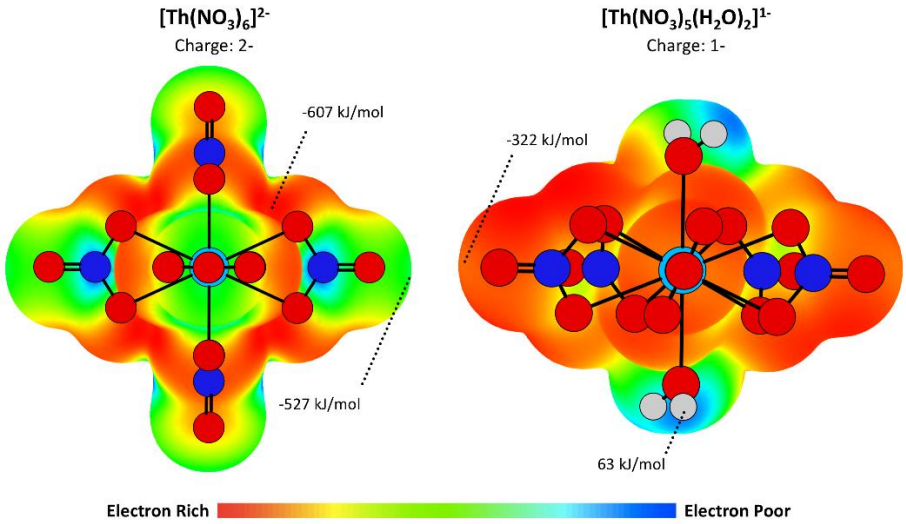

Figure 18. ESP surfaces of anionic Th units found in **1-15**. Regions of interest are highlighted. Surfaces were mapped onto a 0.002 ε/bohr isodensity surface. Color ranges, in kJ/mol, are annotated via the max and min values in the figure.

Table 5. Topographical highlights from ESP surfaces for organic cations in **1**–**15**.

	E_{min} ($^{kJ}/_{mol}$)	E_{max} ($^{kJ}/_{mol}$)	ΔE ($^{kJ}/_{mol}$)	ΔE_{max} - ΔE_H
$[Th(NO_3)_6]^{2-}$	-607	-527	80	-
$[Th(H_2O)_2(NO_3)_5]^{1-}$	-322	63	385	385
$[TerpyH_2]^{2+}$	584	904	320	320
$[PiperH_2]^{2+}$	849	1,090	241	241
[PhthalH]$^{1+}$	224	635	411	
[PhenH]$^{1+}$	244	562	318	
$[4,4'\text{-}BipyH_2]^{2+}$	724	898	174	135
[4-MePyH]$^{1+}$	361	660	299	299
[2-MePyH]$^{1+}$	361	665	304	304
[3-ClPyH]$^{1+}$	309	693	384	
[3,5-DiMePyH]$^{1+}$	349	655	306	306
[3-MePyH]$^{1+}$	364	669	305	305
[PyH]$^{1+}$	427	685	258	

ESP surfaces were also generated for the organic cationic units to complete the record and to rationalize the resistance to speciation in these thorium-nitrate based compounds. The results from these calculations are provided as Supplementary Information (Figure S61). The ESP values for the cationic organic units are all positive, indicating general electron depletion along the surface. We first draw attention to the organic dications as these give rise to the structurally interesting $[Th(H_2O)_2(NO_3)_5]^{1-}$ unit. As expected, these higher charged organic cations feature the greatest electron deficiency with the highest ESP values ranging from 898 kJ/mol $[4,4'\text{-}BipyH_2]^{2+}$ to 1,090 kJ/mol $[PiperH_2]^{2+}$. The large ESP values at the H-N atoms demonstrates strong hydrogen bond donation capabilities for these ions. Within this subgroup, $[PiperH_2]^{2+}$ and $[TerpyH_2]^{2+}$ are distinctly different from $[4,4'\text{-}BipyH_2]^{2+}$ owing to differences in ESP values at the H-C atoms. Findings reveal that $[PiperH_2]^{2+}$ and $[TerpyH_2]^{2+}$ feature the greatest region of relative electron richness (minimum ESP value) at the H-C atoms (849 kJ/mol and 584 kJ/mol, respectively) whereas $[4,4'\text{-}BipyH_2]^{2+}$has the lowest relative ESP value at the center of the aromatic ring (724 kJ/mol). We take this to imply that the H-C atoms of $[PiperH_2]^{2+}$ and $[TerpyH_2]^{2+}$ are much weaker hydrogen bond donors compared to the H-N atom and may not be able to compete energetically. This is not the case for $[4,4'\text{-}BipyH_2]^{2+}$ for which the ESP values at the H-C atoms are much closer in electrostatic potential to the H-N atom at ~763 kJ/mol. The monocations which exclusively give rise to the hexanitrato unit feature much smaller positive potential values, signifying weaker hydrogen bond capacity. For these the H-N atoms have the greatest potential values ranging from 562 kJ/mol $[PhenH]^{1+}$ to 693 kJ/mol $[3\text{-}ClPyH]^{1+}$ and thus are the sites for the strongest hydrogen bond donation in this group. The methyl functional groups have the region of lowest ESP found at the H-C atom. For $[3\text{-}ClPyH]^{1+}$, the lowest ESP region occurs at the Cl atom owing to polarization about the C-Cl bond, a common feature in halogenated pyridines. The $[PhenH]^{1+}$ and $[PhthalH]^{1+}$ cations each have an unprotonated N atom whose free electron pair features the lowest ESP value.

CONCLUSIONS

There is an ongoing need to better understand the factors that impact actinide speciation. As our command of this chemistry develops, we can more reliably predict the chemical behavior of these radionuclides under environmental, waste management, and separations conditions. In this work,

we have shown the synthesis of fifteen different compounds. These complexes were isolated and structurally characterized to show the formation of two unique structural units of the general formulas $[Th(NO_3)_6]^{2-}$ and $[Th(NO_3)_5(H_2O)_2]^{1-}$. Through both experimental and computational means clear thermodynamic sinks for these two molecular units were predicted by the energetic calculations, and clear differences in electron density around the metal center were predicted by the ESP calculations. Due to the limited speciation of the nitrate system, it can be speculated that the nitrates tend to overcome the influence of the cations in driving speciation, resulting in more limited structural diversity with nitrates in comparison to that seen with chlorides. While much remains unknown regarding what specifically drives the precipitation of the $[Th(NO_3)_6]^{2-}$ over the $[Th(NO_3)_5(H_2O)_2]^{1-}$ structural units, it is clear that the presence of counterions, even those that do not directly interact with the metal center drive the formation of anionic structural units. Yet decoupling the competing effects of solution conditions, metal-ligand complexation, and counterion identity remain an ongoing need.

Associated Content

Supplementary Information Available: Synthetic details, crystallographic refinement details, ortep diagrams of compounds, supramolecular packing diagrams, powder X-ray diffraction plots of compounds, Raman and infrared spectra plots of compounds, supramolecular interactions observed in compounds, and computational methods.

This material is available free of charge via the Internet at accession codes: CCDC 2293425-2293439 contains the supplementary crystallographic data for this paper.

Author Information

Corresponding Author*:* *(K.E.K.) Email: kek44@georgetown.edu

ORCID:

Madeline C. Shore: 0000-0002-2090-3595
Aaron D. Nicholas: 0000-0001-9003-2126
Jeffery A. Bertke: 0000-0002-3419-5163
David A. Dixon: 0000-0002-9492-0056
Karah E. Knope: 000-0002-5690-715X

Notes: The authors declare no competing financial interest.

Conflicts of interest

There are no conflicts to declare.

Acknowledgements

The primary source of support for this work is the U.S. Department of Energy, Office of Science, Office of Basic Energy Sciences, Early Career Research Program under Award DE-SC0019190. The computational work was also supported by the U.S. Department of Energy (DOE), Office of Science, Office of Basic Energy Sciences, Chemical Sciences, Geosciences, and Biosciences Division, Heavy Element Chemistry Program, at The University of Alabama (MV, GDM, DAD) through Grant No. DE-SC0018921. D.A.D. thanks the Robert Ramsay Fund at The University of Alabama.

REFERENCES

(1) Shohel, M.; Bustos, J.; Stroscio, G. D.; Sarkar, A.; Nyman, M. Elucidating Actinide-Pertechnetate and Actinide-Perrhenate Bonding via a Family of Th-TcO4 and Th-ReO4 Frameworks and Solutions. *Inorg. Chem.* **2023**, *62* (26), 10450–10460. https://doi.org/10.1021/acs.inorgchem.3c01430.

(2) Silva, R. J.; Nitsche, H. Actinide Environmental Chemistry. *Ract* **1995**, *70–71* (Supplement), 377–396. https://doi.org/10.1524/ract.1995.7071.special-issue.377.

(3) Maher, K.; Bargar, J. R.; Brown, G. E. Environmental Speciation of Actinides. *Inorg. Chem.* **2013**, *52* (7), 3510–3532. https://doi.org/10.1021/ic301686d.

(4) Natrajan, L. S.; Swinburne, A. N.; Andrews, M. B.; Randall, S.; Heath, S. L. Redox and Environmentally Relevant Aspects of Actinide(IV) Coordination Chemistry. *Coord. Chem. Rev.* **2014**, *266–267* (1), 171–193. https://doi.org/10.1016/j.ccr.2013.12.021.

(5) Deblonde, G. J. P.; Lohrey, T. D.; Booth, C. H.; Carter, K. P.; Parker, B. F.; Larsen, Å.; Smeets, R.; Ryan, O. B.; Cuthbertson, A. S.; Abergel, R. J. Solution Thermodynamics and Kinetics of Metal Complexation with a Hydroxypyridinone Chelator Designed for Thorium-227 Targeted Alpha Therapy. *Inorg. Chem.* **2018**, *57* (22), 14337–14346. https://doi.org/10.1021/acs.inorgchem.8b02430.

(6) Thiele, N. A.; Wilson, J. J. Actinium-225 for Targeted α Therapy: Coordination Chemistry and Current Chelation Approaches. *Cancer Biother. Radiopharm.* **2018**, *33* (8), 336–348. https://doi.org/10.1089/cbr.2018.2494.

(7) Dennett, C. A.; Poudel, N.; Simmonds, P. J.; Tiwari, A.; Hurley, D. H.; Gofryk, K. Towards Actinide Heterostructure Synthesis and Science. *Nat. Commun.* **2022**, *13* (1), 13–16. https://doi.org/10.1038/s41467-022-29817-0.

(8) Surbella, R. G.; Ducati, L. C.; Schofield, M. H.; McNamara, B. K.; Pellegrini, K. L.; Corbey, J. F.; Schwantes, J. M.; Autschbach, J.; Cahill, C. L. Plutonium Hybrid Materials: A Platform to Explore Assembly and Metal-Ligand Bonding. *Inorg. Chem.* **2022**, *61* (45), 17963–17971. https://doi.org/10.1021/acs.inorgchem.2c02084.

(9) Hutchison, D. C.; Kravchuk, D. V.; Rajapaksha, H.; Stegman, S.; Forbes, T. Z.; Wilson, R. E. Synthesis of Single Crystal Li2NpO4 and Li4NpO5 from Aqueous Lithium Hydroxide Solutions under Mild Hydrothermal Conditions. *Inorg. Chem.* **2023**, *62* (40), 16564–16573. https://doi.org/10.1021/acs.inorgchem.3c02460.

(10) Rajapaksha, H.; Benthin, G. C.; Kravchuk, D. V; Lightfoot, H.; Mason, S. E.; Forbes, T. Z. Three-Dimensional Noncovalent Interaction Network within $[NpO_2Cl_4]^{2-}$ Coordination Compounds : Influence on Thermochemical and Vibrational Properties. **2023**. https://doi.org/10.1021/acs.inorgchem.3c02502.

(11) Long, B. N.; Beltrán-Leíva, M. J.; Sperling, J. M.; Poe, T. N.; Celis-Barros, C.; Albrecht-Schönzart, T. E. Altering the Spectroscopy, Electronic Structure, and Bonding of Organometallic Curium(III) upon Coordination of 4,4′−bipyridine. *Nat. Commun.* **2023**, *14* (1). https://doi.org/10.1038/s41467-023-39481-7.

(12) Gaiser, A. N.; Celis-Barros, C.; White, F. D.; Beltran-Leiva, M. J.; Sperling, J. M.; Salpage, S. R.; Poe, T. N.; Gomez Martinez, D.; Jian, T.; Wolford, N. J.; et al. Creation of an Unexpected Plane of Enhanced Covalency in Cerium(III) and Berkelium(III) Terpyridyl Complexes. *Nat. Commun.* **2021**, *12* (1), 1–9. https://doi.org/10.1038/s41467-021-27576-y.

(13) Carter, K. P.; Shield, K. M.; Smith, K. F.; Jones, Z. R.; Wacker, J. N.; Arnedo-Sanchez,

L.; Mattox, T. M.; Moreau, L. M.; Knope, K. E.; Kozimor, S. A.; et al. Structural and Spectroscopic Characterization of an Einsteinium Complex. *Nature* **2021**, *590* (7844), 85–88. https://doi.org/10.1038/s41586-020-03179-3.

(14) Sigmon, G. E.; Hixon, A. E. Extension of the Plutonium Oxide Nanocluster Family to Include {Pu 16 } and {Pu 22 }. *Chem. - A Eur. J.* **2019**, *25* (10), 2463–2466. https://doi.org/10.1002/chem.201805605.

(15) Knope, K. E.; Soderholm, L. Solution and Solid-State Structural Chemistry of Actinide Hydrates and Their Hydrolysis and Condensation Products. *Chem. Rev.* **2013**, *113* (2), 944–994. https://doi.org/10.1021/cr300212f.

(16) Henry, M.; Jolivet, J. P.; Livage, J. Aqueous Chemistry of Metal Cations: Hydrolysis, Condensation and Complexation. *Chem. Spectrosc. Appl. Sol-Gel Glas.* **2006**, 153–206. https://doi.org/10.1007/bfb0036968.

(17) Verma, P. K.; Mohapatra, P. K.; Bhattacharyya, A.; Yadav, A. K.; Jha, S. N.; Bhattacharyya, D. Structural Investigations on Uranium(VI) and Thorium(IV) Complexation with TBP and DHOA: A Spectroscopic Study. *New J. Chem.* **2018**, *42* (7), 5243–5255. https://doi.org/10.1039/c7nj04460g.

(18) Jin, G. B.; Lin, J.; Estes, S. L.; Skanthakumar, S.; Soderholm, L. Influence of Countercation Hydration Enthalpies on the Formation of Molecular Complexes: A Thorium-Nitrate Example. *J. Am. Chem. Soc.* **2017**, *139* (49), 18003–18008. https://doi.org/10.1021/jacs.7b09363.

(19) Levin, J. R.; Dorfner, W. L.; Carroll, P. J.; Schelter, E. J. Control of Cerium Oxidation State through Metal Complex Secondary Structures. *Chem. Sci.* **2015**, *6* (12), 6925–6934. https://doi.org/10.1039/c5sc02607e.

(20) Bell, N. L.; Shaw, B.; Arnold, P. L.; Love, J. B. Uranyl to Uranium(IV) Conversion through Manipulation of Axial and Equatorial Ligands. *J. Am. Chem. Soc.* **2018**, *140* (9), 3378–3384. https://doi.org/10.1021/jacs.7b13474.

(21) Tsui, E. Y.; Tran, R.; Yano, J.; Agapie, T. Redox-Inactive Metals Modulate the Reduction Potential in Heterometallic Manganese-Oxido Clusters. *Nat. Chem.* **2013**, *5* (4), 293–299. https://doi.org/10.1038/nchem.1578.

(22) Ryan, A. J.; Ziller, J. W.; Evans, W. J. The Importance of the Counter-Cation in Reductive Rare-Earth Metal Chemistry: 18-Crown-6 Instead of 2,2,2-Cryptand Allows Isolation of [YII(NR2)3]1- and Ynediolate and Enediolate Complexes from CO Reactions. *Chem. Sci.* **2020**, *11* (7), 2006–2014. https://doi.org/10.1039/c9sc05794c.

(23) Macinnes, M. M.; Jones, Z. R.; Li, B.; Anderson, N. H.; Batista, E. R.; Dimucci, I. M.; Eiroa-Lledo, C.; Knope, K. E.; Livshits, M. Y.; Kozimor, S. A.; et al. Using Molten Salts to Probe Outer-Coordination Sphere Effects on Lanthanide(Iii)/(Ii) Electron-Transfer Reactions. *Dalt. Trans.* **2021**, *50* (43), 15696–15710. https://doi.org/10.1039/d1dt02708e.

(24) Estes, S. L.; Qiao, B.; Jin, G. B. Ion Association with Tetra-n-Alkylammonium Cations Stabilizes Higher-Oxidation-State Neptunium Dioxocations. *Nat. Commun.* **2019**, *10* (1), 1–8. https://doi.org/10.1038/s41467-018-07982-5.

(25) A. Sommers, J.; C. Hutchison, D.; P. Martin, N.; Palys, L.; M. Amador, J.; A. Keszler, D.; Nyman, M. Differentiating Zr/HfIV Aqueous Polyoxocation Chemistry with Peroxide Ligation. *Inorg. Chem.* **2021**, *60* (3), 1631–1640. https://doi.org/10.1021/acs.inorgchem.0c03128.

(26) Berger, C.; Marie, C.; Guillaumont, D.; Tamain, C.; Dumas, T.; Dirks, T.; Boubals, N.; Acher, E.; Laszczyk, M.; Berthon, L. Coordination Structures of Uranium(VI) and

Plutonium(IV) in Organic Solutions with Amide Derivatives. *Inorg. Chem.* **2020**, *59* (3), 1823–1834. https://doi.org/10.1021/acs.inorgchem.9b03024.
(27) Wacker, J. N.; Nicholas, A. D.; Vasiliu, M.; Marwitz, A. C.; Bertke, J. A.; Dixon, D. A.; Knope, K. E. Impact of Noncovalent Interactions on the Structural Chemistry of Thorium(IV)-Aquo-Chloro Complexes. *Inorg. Chem.* **2021**, *60* (9), 6375–6390. https://doi.org/10.1021/acs.inorgchem.1c00099.
(28) Blanes-Díaz, A.; Stewart, O.; Vasiliu, M.; Nicholas, A.; Murray, A.; Shore, M.; Dixon, D.; Knope, K. Th(IV) Bromide Complexes: A Homoleptic Aqua Ion and a Novel $Th(H_2O)_4Br_4$ Structural Unit. *Cryst. Growth Des. 22* (7), 4375–4381. https://doi.org/10.1021/acs.cgd.2c00353.
(29) Wacker, J. N.; Vasiliu, M.; Huang, K.; Baumbach, R. E.; Bertke, J. A.; Dixon, D. A.; Knope, K. E. Uranium(IV) Chloride Complexes: UCl62- and an Unprecedented U(H2O)4Cl4 Structural Unit. *Inorg. Chem.* **2017**, *56* (16), 9772–9780. https://doi.org/10.1021/acs.inorgchem.7b01293.
(30) Wacker, J. N.; Han, S. Y.; Murray, A. V.; Vanagas, N. A.; Bertke, J. A.; Sperling, J. M.; Surbella, R. G.; Knope, K. E. From Thorium to Plutonium: Trends in Actinide(IV) Chloride Structural Chemistry. *Inorg. Chem.* **2019**, *58* (16), 10578–10591. https://doi.org/10.1021/acs.inorgchem.9b01279.
(31) Rand, M.; Fuger, J.; Grenthe, I.; Neck, V.; Rai, D. Chemical Thermodynamics of Thorium. *NEA - Nucl. Energy Agency* **2009**, *11* (9), 1–945.
(32) Bhattacharjee, R.; Miró, P. Aqueous Speciation of Tetravalent Actinides in the Presence of Chloride and Nitrate Ligands. *Inorg. Chem.* **2022**, *61* (37), 14718–14725. https://doi.org/10.1021/acs.inorgchem.2c02064.
(33) Wickleder, M. S.; Fourest, B.; Dorhout, P. K. THORIUM. **1885**.
(34) Williams, R. Hans Reich's Collection.PKa Values in Water Compilation. *ACS Div. Org. Chem.* **2021**, 1–33.
(35) SADABS. Bruker AXS Inc: Madison, WI, USA 2008.
(36) Sheldrick, G. M. Crystal Structure Refinement with SHELXL. *Acta Crystallogr. Sect. C Struct. Chem.* **2015**, *71* (Md), 3–8. https://doi.org/10.1107/S2053229614024218.
(37) Boucher, G. Book Reviews: Book Reviews. *Crit. Sociol.* **2011**, *37* (4), 493–497. https://doi.org/10.1177/0261018311403863.
(38) Lecklider, T. Maintainng a Heathy Rhythm. *EE Eval. Eng.* **2011**, *50* (11), 36–39.
(39) Becke, A. D. Density-Functional Thermochemistry. III. The Role of Exact Exchange. *J. Chem. Phys.* **1993**, *98* (7), 5648–5652. https://doi.org/10.1063/1.464913.
(40) Kendall, R. A.; Dunning, T. H.; Harrison, R. J. Electron Affinities of the First-Row Atoms Revisited. Systematic Basis Sets and Wave Functions. *J. Chem. Phys.* **1992**, *96* (9), 6796–6806. https://doi.org/10.1063/1.462569.
(41) Peterson, K. A. Correlation Consistent Basis Sets for Actinides. I. the Th and U Atoms. *J. Chem. Phys.* **2015**, *142* (7). https://doi.org/10.1063/1.4907596.
(42) Frisch, M.; Trucks, G.; Schlegel, H.; Scuseria, G.; Robb, M.; Cheeseman, J.; Scalmani, G.; Barone, V.; Petersson, G.; Nakatsuji, H.; al., e. *GAUSSIAN16.*; Gaussian Inc.: Wallingford, CT, USA., 2016.
(43) Ribeiro, R. F.; Marenich, A. V.; Cramer, C. J.; Truhlar, D. G. Use of Solution-Phase Vibrational Frequencies in Continuum Models for the Free Energy of Solvation. *J. Phys. Chem. B* **2011**, *115* (49), 14556–14562. https://doi.org/10.1021/jp205508z.
(44) Purvis, G. D.; Bartlett, R. J. A Full Coupled-Cluster Singles and Doubles Model: The

Inclusion of Disconnected Triples. *J. Chem. Phys.* **1982**, *76* (4), 1910–1918. https://doi.org/10.1063/1.443164.
(45) Raghavachari, K.; Trucks, G. W.; Pople, J. A.; Head-gordon, M. Krishnan RAGHAVACHARI, Gary W. TRUCKS. *Chem. Phys. Lett.* **1989**, *157* (6), 479–483.
(46) Watts, J. D.; Gauss, J.; Bartlett, R. J. Coupled-Cluster Methods with Noniterative Triple Excitations for Restricted Open-Shell Hartree-Fock and Other General Single Determinant Reference Functions. Energies and Analytical Gradients. *J. Chem. Phys.* **1993**, *98* (11), 8718–8733. https://doi.org/10.1063/1.464480.
(47) Bartlett, R. J.; Musiał, M. Coupled-Cluster Theory in Quantum Chemistry. *Rev. Mod. Phys.* **2007**, *79* (1), 291–352. https://doi.org/10.1103/RevModPhys.79.291.
(48) Møller, P. MP2 Notes. *Eur. J. Cardio-thoracic Surg.* **1934**, *53* (6), 1237–1243.
(49) Pople, J. A.; Binkley, J. S.; Seeger, R. Theoretical Models Incorporating Electron Correlation. *Int. J. Quantum Chem.* **1976**, *10* (10 S), 1–19. https://doi.org/10.1002/qua.560100802.
(50) Werner, H.-J.; Knowles, P. J.; Knizia, G.; Manby, F. R.; Schütz, M.; Celani, P.; Györffy, W.; Kats, D.; Korona, T.; Lindh, R. . et al. MOLPRO, version 2020.1, a package of ab initio programs.
(51) Werner, H. J.; Knowles, P. J.; Manby, F. R.; Black, J. A.; Doll, K.; Heßelmann, A.; Kats, D.; Köhn, A.; Korona, T.; Kreplin, D. A.; et al. The Molpro Quantum Chemistry Package. *J. Chem. Phys.* **2020**, *152* (14). https://doi.org/10.1063/5.0005081.
(52) 42- 292. **2005**, *292*, 56126.
(53) Book Reviews. *Byron J.* **2006**, *34* (2), 190–200. https://doi.org/10.3828/bj.34.2.12.
(54) Klamt, A.; Schüürmann, G. COSMO: A New Approach to Dielectric Screening in Solvents with Explicit Expressions for the Screening Energy and Its Gradient. *J. Chem. Soc. Perkin Trans. 2* **1993**, No. 5, 799–805. https://doi.org/10.1039/P29930000799.
(55) Marwitz, A. C.; Nicholas, A. D.; Breuer, L. M.; Bertke, J. A.; Knope, K. E. Harnessing Bismuth Coordination Chemistry to Achieve Bright, Long-Lived Organic Phosphorescence. *Inorg. Chem.* **2021**, *60* (21), 16840–16851. https://doi.org/10.1021/acs.inorgchem.1c02748.
(56) Nicholas, A. D.; Halli, R. N.; Garman, L. C.; Cahill, C. L. Low-Dimensional Hybrid Indium/Antimony Halide Perovskites: Supramolecular Assembly and Electronic Properties. *J. Phys. Chem. C* **2020**, *124* (47), 25686–25700. https://doi.org/10.1021/acs.jpcc.0c07268.
(57) Byrne, N. M.; Schofield, M. H.; Nicholas, A. D.; Cahill, C. L. Bimetallic Uranyl/Cobalt(Ii) Isothiocyanates: Structure, Property and Spectroscopic Analysis of Homo- And Heterometallic Phases. *Dalt. Trans.* **2021**, *50* (26), 9158–9172. https://doi.org/10.1039/d1dt01464a.
(58) Nicholas, A. D.; Garman, L. C.; Albano, N.; Cahill, C. L. Insight on Noncovalent Interactions and Orbital Constructs in Low-Dimensional Antimony Halide Perovskites. *Phys. Chem. Chem. Phys.* **2022**, *24* (25), 15305–15320. https://doi.org/10.1039/d2cp01996e.
(59) Janiak, C. A Critical Account on N-n Stacking in Metal Complexes with Aromatic Nitrogen-Containing Ligands. *J. Chem. Soc. Dalt. Trans.* **2000**, No. 21, 3885–3896. https://doi.org/10.1039/b003010o.
(60) Mathur, J. N.; Murali, M. S.; Nash, K. L. Actinide Partitioning-A Review. *Solvent Extr. Ion Exch.* **2001**, *19* (3), 357–390. https://doi.org/10.1081/SEI-100103276.

(61) Katz, J. J.; Seaborg, G. T. *Actinide and Transactinide Elements*; 2010.
(62) Cotton, S. *Lanthanide and Actinide Chemistry*; 2006. https://doi.org/10.1002/0470010088.
(63) Amani, V.; Tayebee, R. Synthesis, Characterization, Thermal Analyses and Crystal Structure of a New Thorium(IV) Nitrate Complex: [Phen.H]2[Th(NO3) 6].2H2O. *Synth. React. Inorganic, Met. Nano-Metal Chem.* **2013**, *43* (9), 1118–1123. https://doi.org/10.1080/15533174.2012.756025.
(64) Ferraro, J. R.; Katzin, L. I.; Gibson, G. The Reaction of Thorium Nitrate Tetrahydrate with Nitrogen Oxides. Anhydrous Thorium Nitrate. *J. Am. Chem. Soc.* **1955**, *77* (2), 327–329. https://doi.org/10.1021/ja01607a023.
(65) Spirlet, M. R.; Rebizant, J.; Apostolidis, C.; Kanellakopulos, B.; Dornberger, E. Structure of Bis(Ammonium) Hexanitratoplutonium(IV) and Bis(Ammonium) Hexanitratothorium(V). *Acta Crystallogr. Sect. C Cryst. Struct. Commun.* **1992**, *48* (7), 1161–1164. https://doi.org/10.1107/s0108270191006753.
(66) Wacker, J. N.; Nicholas, A. D.; Vasiliu, M.; Marwitz, A. C.; Bertke, J. A.; Dixon, D. A.; Knope, K. E. Impact of Noncovalent Interactions on the Structural Chemistry of Thorium(IV)-Aquo-Chloro Complexes. *Inorg. Chem.* **2021**, *60* (9), 6375–6390. https://doi.org/10.1021/acs.inorgchem.1c00099.
(67) Wilson, R. E.; Schnaars, D. D.; Andrews, M. B.; Cahill, C. L. Supramolecular Interactions in $PuO_2Cl_4^{2-}$ and $PuCl_6^{2-}$ Complexes with Protonated Pyridines: Synthesis, Crystal Structures, and Raman Spectroscopy. *Inorg. Chem.* **2014**, *53* (1), 383–392. https://doi.org/10.1021/ic4023294.
(68) Surbella, R. G.; Ducati, L. C.; Autschbach, J.; Pellegrini, K. L.; McNamara, B. K.; Schwantes, J. M.; Cahill, C. L. Plutonium Chlorido Nitrato Complexes: Ligand Competition and Computational Metrics for Assembly and Bonding. *Chem. Commun.* **2018**, *54* (85), 12014–12017. https://doi.org/10.1039/C8CC05578E.
(69) Kravchuk, D. V.; Blanes Diaz, A.; Carolan, M. E.; Mpundu, E. A.; Cwiertny, D. M.; Forbes, T. Z. Uranyl Speciation on the Surface of Amidoximated Polyacrylonitrile Mats. *Inorg. Chem.* **2020**, *59* (12), 8134–8145. https://doi.org/10.1021/acs.inorgchem.0c00440.
(70) Bjorklund, J. L.; Pyrch, M. M.; Basile, M. C.; Mason, S. E.; Forbes, T. Z. Actinyl-Cation Interactions: Experimental and Theoretical Assessment of [Np(vi)O2Cl4]2- and [U(vi)O2Cl4]2- Systems. *Dalt. Trans.* **2019**, *48* (24), 8861–8871. https://doi.org/10.1039/c9dt01753d.
(71) Larkin, P. J. *Infrared and Raman Spectroscopy: Principles and Spectral Interpretation*; 2017. https://doi.org/10.1016/C2015-0-00806-1.